Probing Short Range Correlations

BM@N Project

List of organizations and participants

Russia: Joint Institute for Nuclear Research – JINR (Dubna) the BM@N collaboration

Israel: Tel Aviv University

Germany: TUD and GSI

USA: FIU, MIT, ODU, PSU

FRANCE: CEA

Spokespersons:

Or Hen (MIT), Thomas Aumann (TUD, GSI),

Mikhail Kapishin (JINR), Eli Piasetzky (TAU)

Coordinators:

Georgios Laskaris (MIT and TAU), Anatoly Litvinenko (JINR),

Maria Patsyuk (MIT)

Theoretical Support:

Leonid Frankfurt (TAU), Misak Sargsian (FIU), Mark Strikman (PSU)

Abstract

We propose to study Short Range Correlations (SRC) in ^{12}C via hard scattering in inverse kinematics. The proposed measurement will use a ^{12}C beam at 4 GeV/c/u and the BM@N beam line. We propose to knockout a proton from an SRC pair in the carbon nucleus and detect it in coincidence with the target-scattered proton. The proton knockout reaction, $p(^{12}C,2p)X$, will be carried out at large momentum transfer ($|s, t, u|>2$ $(GeV/c)^2$) and a center-of-mass scattering angle around 90^o. By triggering on the coincidence detection of the two protons from the $p(^{12}C,2p)X$ reaction, we also propose to detect in coincidence the recoil partner nucleon emitted in the hard breakup of the SRC pair, as well as the spectator A-2 system. The knockout protons and spectator nuclear fragments will be detected using the existing BM@N detectors. Recoil nucleons will be detected using the NeuLAND neutron detector. This is a pioneering measurement that can only be performed at the JINR Nuclotron in Dubna.

Table of Content

1 Scientific Motivation

The stability of atomic nuclei is the result of a delicate interplay between the long-range attraction that binds nucleons and the short-range repulsion that prevents the collapse of the system. In between, the dominant scalar part of the nucleon-nucleon (NN) force almost vanishes and the interaction is dominated by the tensor force, which depends on the spin orientations and the relative orbital angular momentum of the nucleons.

Already in a 1953 Scientific American journal article, Hans Bethe claimed that probably more man-hours had been devoted to understanding the nucleon-nucleon interaction and how it forms atomic nuclei than to any other scientific question in the history of mankind. Even today, more than 60 years later, our theoretical and experimental knowledge of the short-range part of NN interaction is very limited.

Recent measurements of Short Range Correlations (SRCs) in nuclei probe the tensor part of the NN force and even start to approach the repulsive part by studying the isospin decomposition of SRC pairs. The experiment proposed here intends to: (A) verify the previous phenomenological findings with different reaction/kinematics and (B) allow a first observation of the A-2 system left after the hard breakup of the SRC pair from the ^{12}C nucleus. The use of a nuclear beam and a hard-knockout reaction in inverse kinematics can be a breakthrough in SRC research and can open the way to the development of a new experimental program. In particular, these measurements will enable future studies of SRCs in nuclei far from stability using radioactive beams and will make accessible detailed information on the origin and formation process of SRC pairs through direct measurements of the A-2 system (with gamma spectroscopy and other techniques).

Recent high-momentum-transfer triple-coincidence ^{12}C(e,e'pN) and ^{12}C(p,2pn) measurements [1-4] have shown that nucleons in the nuclear ground state form nucleon pairs with large relative momentum and small center-of-mass (CM) momentum, where large and small are relative to the Fermi momentum of the nucleus (k_F). We refer to these pairs as short-range correlated (SRC) pairs [5-7]. In the range of missing-momentum (the knocked-out proton's pre-scatter momentum in the absence of re-interactions) from 300–600 MeV/c, these pairs were found to dominate the nuclear wave function, with neutron-proton (np) pairs nearly 20 times more prevalent than proton-proton (pp) pairs, and by inference neutron-neutron (nn) pairs (see figure 1). The strong preference for np pairs is due to the dominance of the tensor part of the NN interaction at the probed sub-fm distances [8-10]. These observations were also confirmed in recent measurements on heavier nuclei reaching all the way up to ^{208}Pb [16].

From a theoretical standpoint, the dominance of np-SRC pairs over pp-SRC pairs was primarily studied by examining state-of-the-art ab-initio calculations of pairs momentum distribution functions for different nuclei as a function of the relative momentum between

the nucleons in the pair, $q = (k_1 - k_2)/2$. One such calculation is shown in figure 2 where the dominance of np pairs at high relative pair momenta is clearly evident.

The tensor part of the nucleon-nucleon force is proportional to S, the total spin of the pair. As such, the tensor force prefers S = 1 states (spin-symmetric states having two spins pointing in the same direction) over the S = 0 (the equivalent spin-asymmetric states). Because SRC pairs are mainly in a relative S-state or D-state (even L, symmetric configuration) their isospin must be even (asymmetric) due to the Pauli principle. As a result, the tensor force affects np-SRCs, which have an asymmetric isospin component, while the pp-SRC (or nn-SRC) pairs are much less affected.

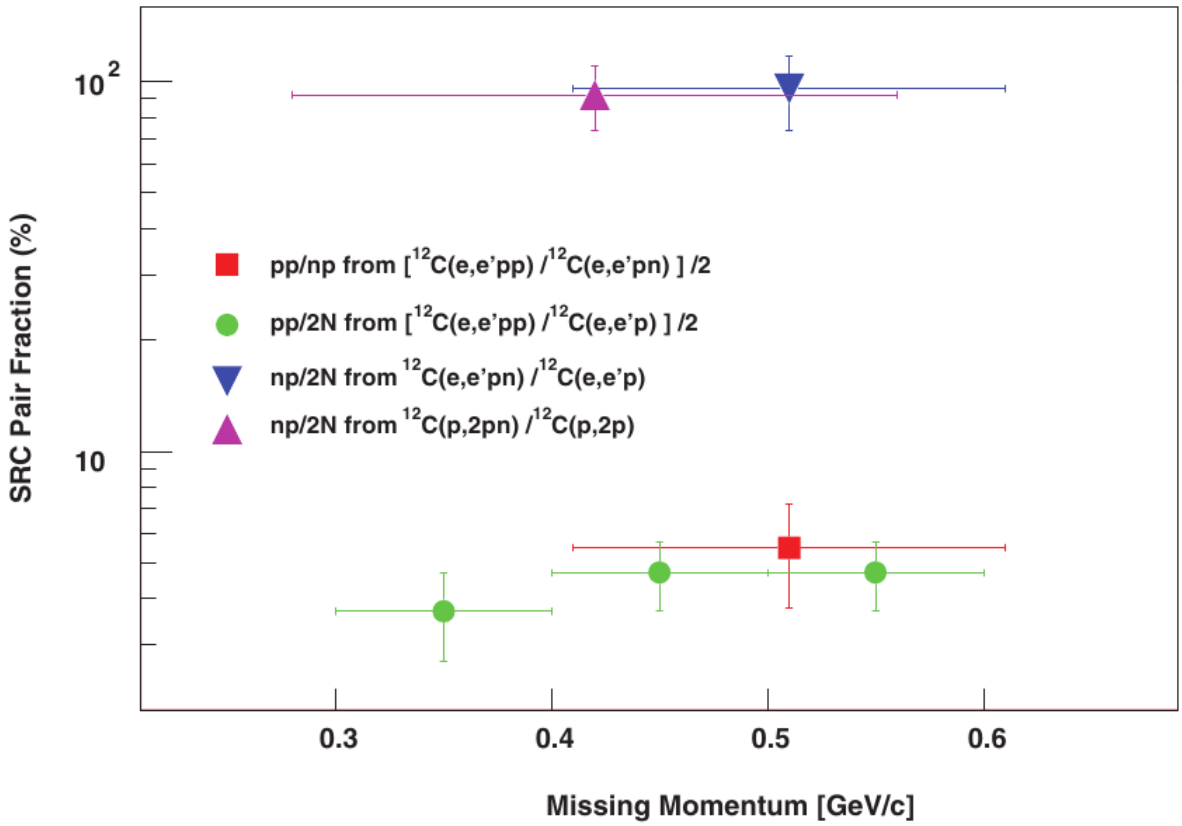

Figure 1: The fractions of correlated pair combinations in carbon as obtained from the ^{12}C(e,e'pp) and ^{12}C(e,e'pn) reactions measured at JLab [1,2] as well as from previous, ^{12}C(p,2pn) data from BNL [3,4].

It should be pointed out that normally the tensor part of the NN interaction is small compared to the dominant scalar part. However, it becomes important in the region where the scalar force approaches zero (~0.75 fm). Figure 3 shows the schematic behavior of the scalar part of the nucleon-nucleon potential, with the region where we expect to measure effect of tensor part of the nucleon-nucleon interaction depicted by a red ellipse.

The association of the small ^{12}C(e,e'pp) / ^{12}C(e,e'pn) ratio at (e,e'p) missing momenta of 300 - 600 MeV/c, with dominance of the NN tensor force, leads naturally to the quest for

increasing missing momenta. This allows the search for pairs at distances in which the nuclear force changes from being predominantly tensor to the essentially unexplored repulsive interaction.

In a recent publication, a simultaneous measurement of the ^{4}He(e,e'p), ^{4}He(e,e'pp) and ^{4}He(e,e'pn) reactions at (e,e'p) missing momenta from 400 to 830 MeV/c was reported. The measurements were motivated by the attempt to study the transition between the tensor-dominated regime to the short-range repulsive (and presumably scalar) nucleon-nucleon force, using the isospin decomposition of 2N-SRCs.

The experiment was performed in Hall A of the Thomas Jefferson Laboratory (JLab) using a 4.5 GeV electron beam and two high resolution, small solid angle, spectrometers that detected the scattered electron and knocked-out proton in coincidence. The kinematical settings of the spectrometers were chosen to cover a missing-momentum range of 400-830 MeV/c. For highly correlated pairs, the missing momentum of the A(e,e'p) reaction is expected to be balanced almost entirely by a single recoiling nucleon. A large acceptance spectrometer (BigBite) and a neutron detector (HAND) with matching acceptances were used to detect correlated recoiling protons or neutrons. The results of these measurements are shown in figure 4 (adapted from [11]).

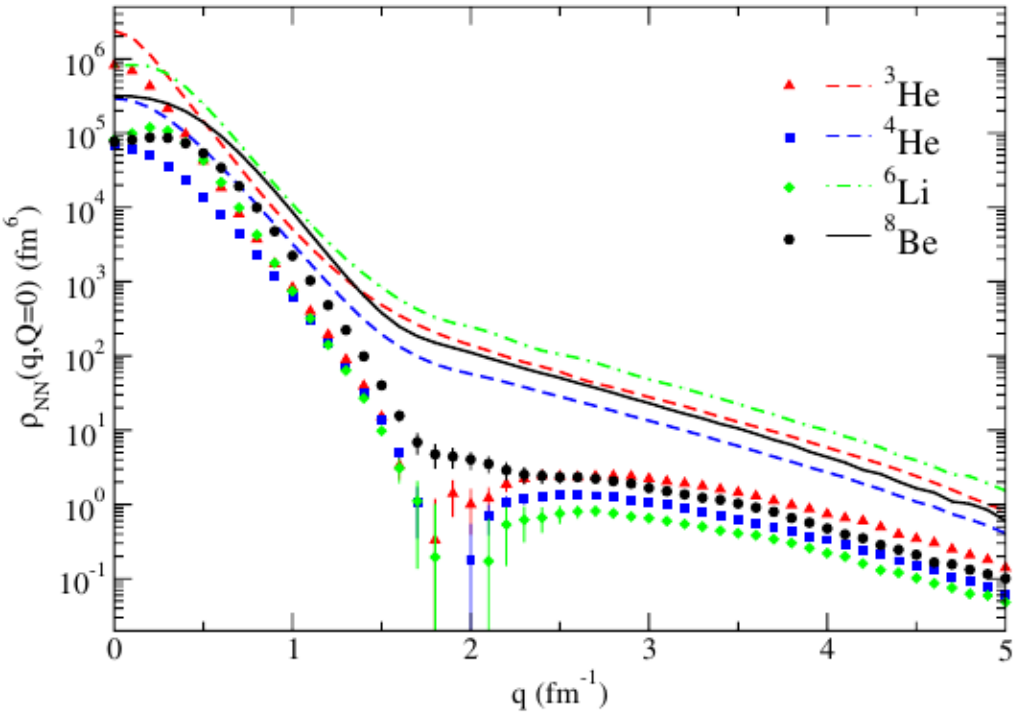

Figure 2: The momentum distribution for np (lines) and pp (symbols) pairs in various nuclei as a function of the relative momentum of the nucleons in the pair (q) from Ref. [8]. The calculations assume pairs at rest (i.e. pair CM momentum Q = 0).

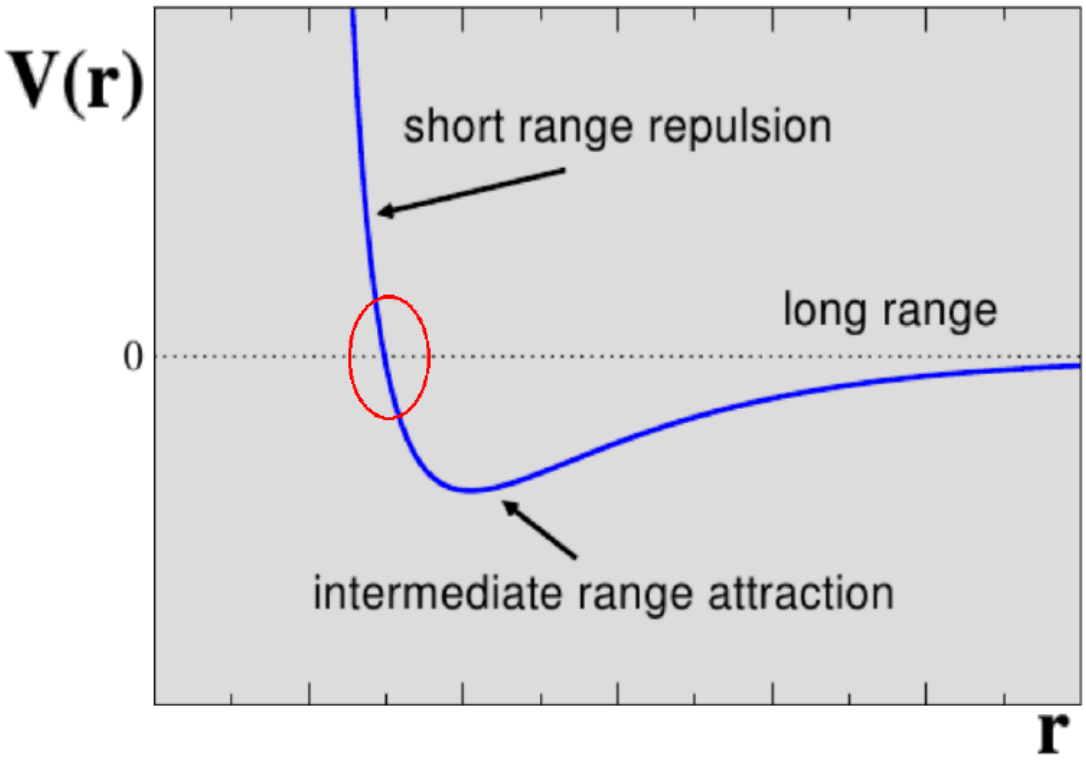

Figure 3: Schematic presentation of scalar part of the NN potential as function of distance between nucleons. Red ellipse present the region, were we expect to measure the effect of the tensor part of the force.

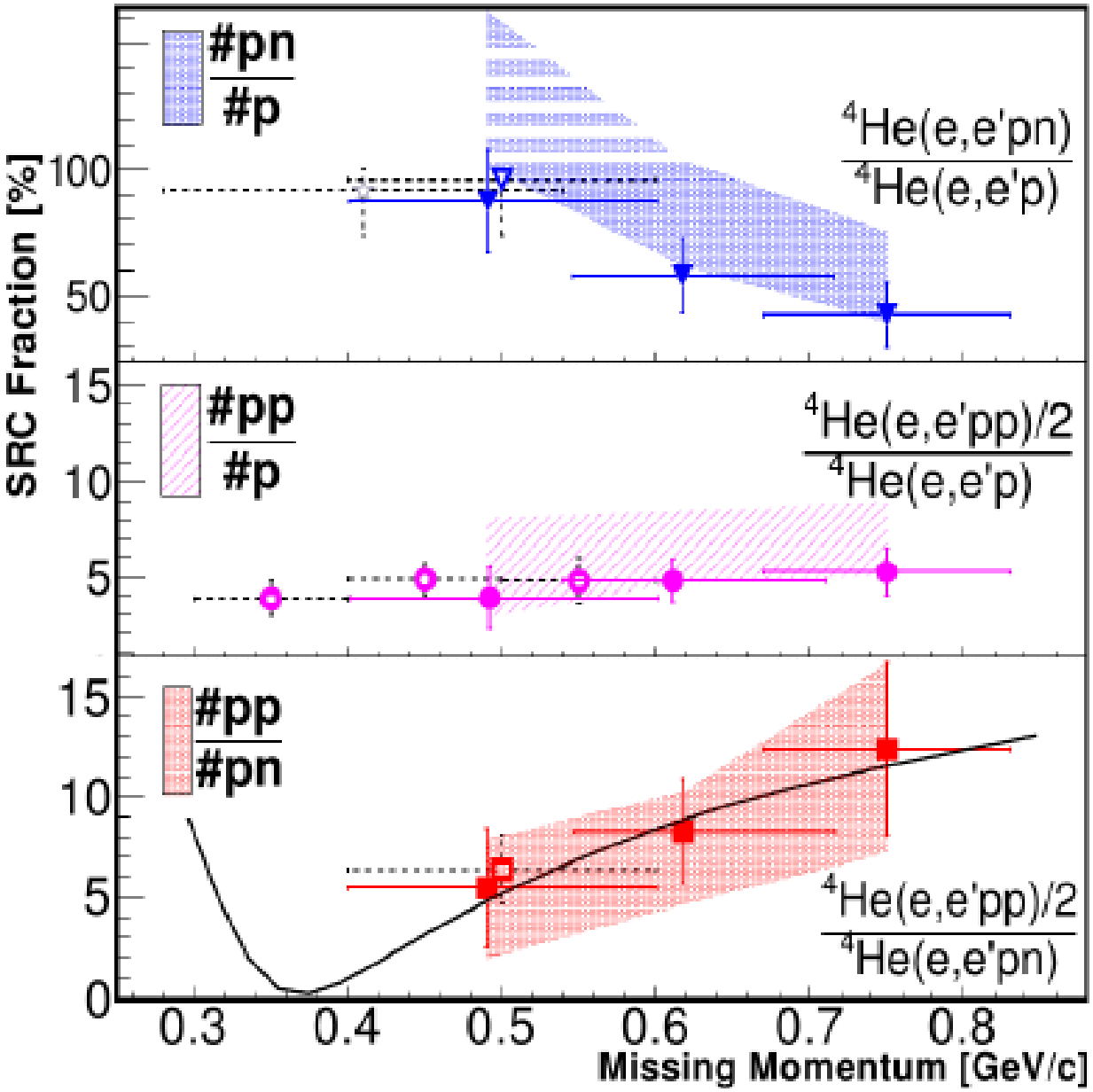

Figure 4: Lower panel: The measured ratios ^{4}He(e, e'pp)/^{4}He(e, e'pn) shown as solid symbols, as a function of the ^{4}He(e, e'p) missing momentum. The bands represent the data corrected for FSI to obtain the pair ratios, see Ref. [12] for details. Also shown are calculations using the momentum distribution of Ref. [10] for pairs with weighted-average CM momentum (**solid black line**). The middle panel shows the measured ^{4}He(e, e'pp)/ ^{4}He(e, e'p) and extracted #pp=#p ratios. The upper panel shows the measured ^{4}He(e, e'pn)/^{4}He(e, e'p) and extracted #pn=#p ratios. The ratios for ^{12}C are shown as empty symbols with dashed bars. The empty star in the upper panel is the BNL result [4] for ^{12}C(p, 2pn)/^{12}C(p, 2p).

The data shown in figure 4 are compared to two-nucleon momentum distributions calculated for the ground state ^{4}He wave function using variational Monte-Carlo and a realistic Hamiltonian with Argonne V18 and Urbana X potentials [10]. The solid (**black**) curve was obtained by weighting the calculations according to the CM momentum of the pair (Q). The calculation with Q = 0, which agrees quantitatively with the Perugia group calculation [13], differs only slightly from the weighted average shown in the plot.

In figure 5 the calculated and measured proton-proton (pp) to proton-neutron (pn) pairs density ratio in ^{4}He is shown as a function of their relative momentum. The experimental data are obtained from [11]. The calculated pair density ratio is shown as a function of the relative pair momentum and is obtained by integrating up to maximum CM momentum, Q_{max}, that varies from zero to infinity. As can be seen, as long as the maximal CM momentum is smaller than k_F, the calculated ratio describes well the experimental data. The dash line is a contact formalism based calculation that assumes SRC pairs can be described by a function that depends on the CM momentum (Q) times a universal two-body function that depends only on the pair relative momentum (q). The later assumption (factorization) is demonstrated well in the figure and discussed in details in Ref. [14]. It is the base for our ability to relate the SRC isospin to the NN interaction at short distances.

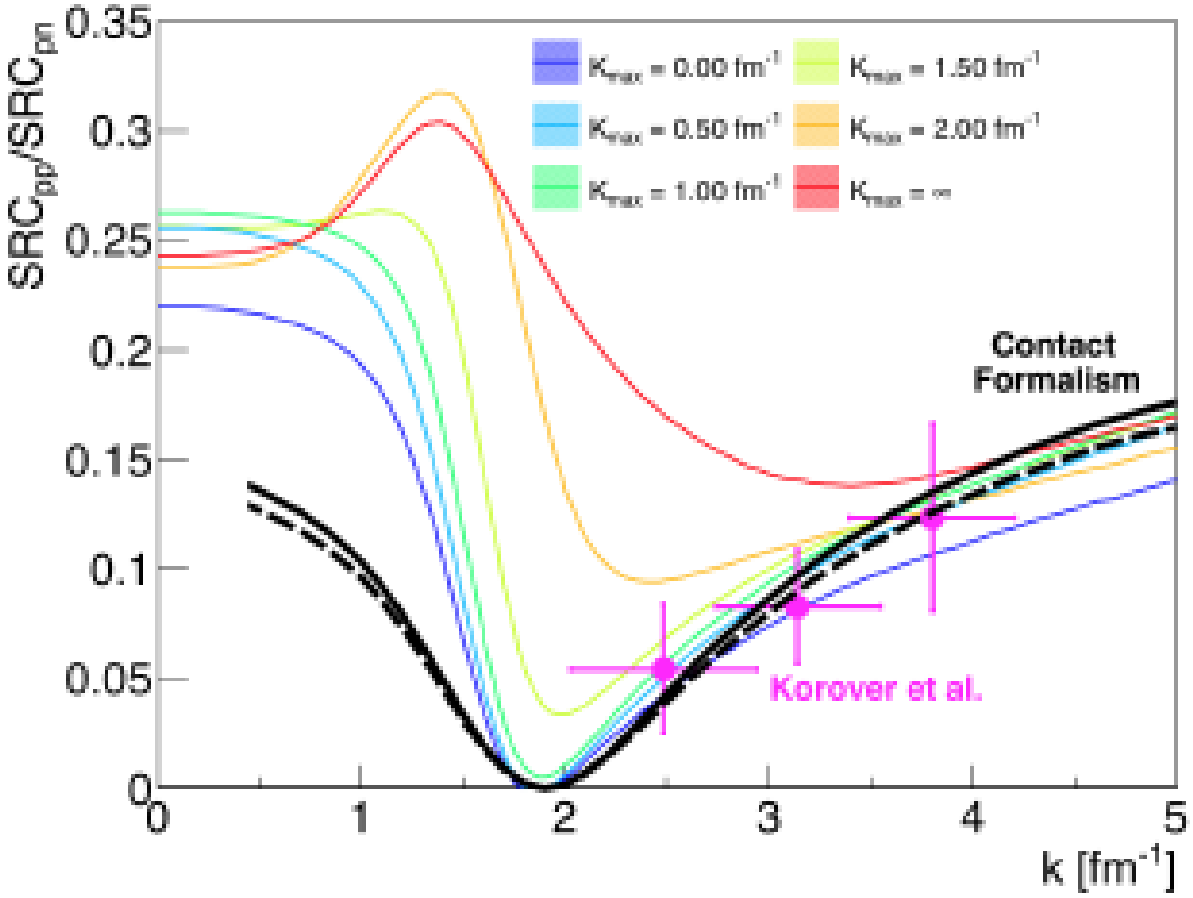

Figure 5: The ratio of proton-proton to proton-neutron SRC pairs in ^{4}He as a function of the pair momentum extracted from ^{4}He(e,e'pN) measurements [11]. The colored lines show the equivalent ab-initio two-body momentum density ratio, integrated over the c.m. momentum from 0 to Q_{max} that varies from zero to infinity [15]. The solid (dashed) **black** line is a contact theory prediction of [14].

There are interesting implications for SRCs in asymmetric nuclei. In neutron-rich nuclei, without SRC pairs, neutrons, as the majority species, should have a higher Fermi momentum and thus a higher average momentum and kinetic energy compared to the minority protons. However, if the high-momentum tail is dominated by np-pairs then there should be equal numbers of protons and neutrons with momentum, k, greater than k_F. In this case, in neutron-rich nuclei the np SRC pairs should increase the average proton momentum more than that of the neutrons and may even result in protons having higher average kinetic energy than neutrons [16,17]. This scenario is referred to as "inversion of the kinetic energy sharing".

In a recent JLab data mining analysis project [18] we directly studied the isospin decomposition of the nucleon high-momentum tail in nuclei by simultaneously measuring hard QE electron scattering off protons and neutrons using the A(e,e'p) and A(e,e'n) reactions respectively for A = ^{12}C, ^{27}Al, ^{56}Fe, and ^{208}Pb nuclei. The simultaneous measurement of both proton and neutron knockout is a unique feature of this work that allowed direct comparisons their properties using minimal assumptions. The data (1) quantify the relative fractions of high-momentum protons and neutrons, (2) confirm the np-SRC dominance of the high-momentum tail in medium and heavy nuclei, and (3) indicate that the nucleon kinetic energy sharing is inverted in heavy nuclei.

Recently, a simultaneous measurement of the proton-knockout (e,e'p) and neutron-knockout (e,e'n) reactions was done in two kinematical settings, corresponding to electron scattering off nucleons from a SRC pair ($k>k_F$) or from the nuclear mean field ($k<k_F$). Using these event samples, the A(e,e'n)/A(e,e'p) cross-section ratio for each kinematics was extracted, see figure 6.

To verify the neutron detection efficiency, detector acceptance corrections, and event selection method, we first extracted for ^{12}C the SRC and mean-field neutron-to-proton knockout reduced cross-section ratios: [^{12}C(e,e'n)/$\sigma_{e\text{-}n}$] / [^{12}C(e,e'p)/$\sigma_{e\text{-}p}$] (i.e. measured cross-sections divided by the known elementary electron-proton $\sigma_{e\text{-}p}$ and electron-neutron $\sigma_{e\text{-}n}$ cross-sections). These cross-section ratios are each consistent with unity, as expected for a symmetric nucleus.

For the other measured nuclei, the n/p mean-field reduced cross-section ratios grow approximately as N/Z, as expected from simple nucleon counting. However, the SRC ratios are consistent with unity for all measured nuclei, just as expected from np-pair dominance. Even in asymmetric nuclei with many more neutrons, the high-momentum tail is equally populated with proton and neutrons.

To determine whether the observed effect is large enough to invert the kinetic energy sharing in heavy neutron-rich nuclei, we use a simple phenomenological (i.e. experiment-based) np-dominance model to describe the momentum distribution of protons and neutron and calculate their average kinetic energies [16]. The model uses the mean-field momentum distributions from one of three different models [16] and a deuteron-like high-momentum tail, scaled by the measured fraction of high-momentum nucleons in nuclei [19-21]. For example, in the case of ^{208}Pb, where 20% of the 208 nucleons have high initial momentum. our model assumes that there are 21 high-momentum protons and 21 high-momentum neutrons. This implies that the high-momentum proton fraction is 21/82 ~ 25% and the corresponding neutron fraction is 21/128 ~ 17%. In contrast to nuclear mean-field predictions, we find that the inclusion of a np-dominant high-momentum tail leads to a neutron-to-proton average kinetic energy ratio ($<E_{kin}^{n}>/<E_{kin}^{p}>$) that decreases with neutron excess, indicating that on average protons move faster than neutrons in neutron-rich nuclei (figure 6). Thus, the data strongly supports kinetic energy inversion:

the minority protons move faster on average than the majority neutrons in asymmetric nuclei.

In conclusion, the simultaneous measurement of electro-induced proton (e,e'p) and neutron (e,e'n) knockout at low- and high-initial momentum from nuclei, show that the high momentum tail of any nucleus ($k>k_F$) is occupied by an equal number of protons and neutrons. In the low-initial momentum region ($k<k_F$) the ratio of neutrons to protons is about N/Z, as expected from simple nucleon counting. This measurement implies that in neutron-rich nuclei, the average proton (minority) momentum kinetic energy is higher than the average neutron momentum kinetic energy (majority). This data stands in contrast to the predictions of current models of medium and heavy nuclei and presents a challenge to future calculations.

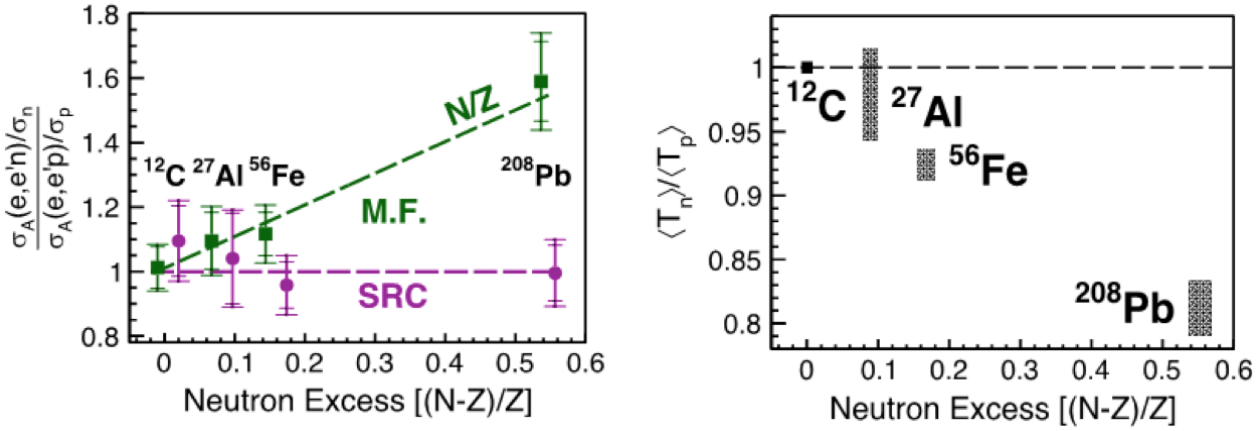

Figure 6: Left: the A(e,e'p)/A(e,e'n) reduced cross-section ratio mean-field (**green**) and SRC (purple) events (left). The dashed lines are simple model predictions for the N/Z neutron excess dependence of the Mean-Field nucleons and the independence of neutron excess of the SRC nucleons. Right: the ratio of the neutron to proton average kinetic energy, as obtained from the np-SRC dominance model, as a function of the neutron excess, indicating that protons move faster than neutrons in neutron rich nuclei.

1.1 Description of the Proposed Research

We propose here a new experimental approach to SRC study via hard inverse and complete kinematics measurements. Inverse kinematics was used to study the equivalent of exclusive quasi-free proton knockout using ^{12}C beam energy of less than 0.5 GeV/u [22]. Here, using the BM@N beam line and equipment and the NeuLAND large acceptance neutron detector from GSI, we extend the inverse kinematics measurement to higher energy, larger momentum transfer, and larger missing momentum and add to it the detection of the recoil partner in the correlation.

We propose to measure simultaneously the following triple and 4- fold coincidence reactions:

(1) $^{12}C + p \rightarrow {}^{11}B + pp$

(2) $^{12}C + p \rightarrow {}^{10}B + pp$ + X (np-SRC)

(3) $^{12}C + p \rightarrow {}^{10}Be + pp$ + X (pp-SRC)

(4) $^{12}C + p \rightarrow {}^{10}B + pp + n$ (np-SRC)

(5) $^{12}C + p \rightarrow {}^{10}Be + pp + p$ (pp-SRC).

These reactions will be measured with a large (p,2p) missing momentum so that the event sample will be dominated by 2N-SRC. We propose to extract from the measured yield, after corrections for acceptance, efficiencies etc. the ratios of:

- $np-SRC \,/\, pp-SRC$ [from reactions (2) and (4) (3) and(5)]
- $np-SRC \,/\, (p, pp)$ [from reactions (2) and (4) and(1)]
- $pp-SRC \,/\, (p, pp)$ [from reactions (2) and (4) and(1)]

The results are to be compared with the electron scattering, high energy proton induced study of SRC and calculations.

1.2 Objectives

Identify 2N-SRC events in inverse kinematics

Study the isospin decomposition of the 2N-SRC

Study the A-2 nuclear system left after the 2N-SRC removal

1.3 Theoretical Support

One of the advantages of high energy probes is simplification of the scattering process theoretical description. This is due to suppression of the pion exchange and intermediate resonance production processes and the applicability of Eikonal approximation in the calculation of the initial and final state small angle (soft) re-interactions.

The important condition for applicability of the high-energy approximation is the requirement that the produced mass in the elementary pN process exceeds the mass for the deep inelastic regime, i.e. W = $\sqrt{s_p N}$ >2.5 GeV. In this case, the closure approximation allows to sum all the contributions of the intermediate resonances. The practical application of such approximation is the use of the phenomenological parameterization for the hard pN->pN scattering cross section without considering excitation of intermediate resonances with further re-scattering. This approximation is successfully applied to hard

nuclear processes such as in A(p,2p)X and A(p,2pn)X reactions [23,24,4] in which s_{pp}>12 (GeV/c)^2 as well as hard photodisintegration of the few-nucleon systems in A(γ, pn/p)X at $\sqrt{s_\gamma N}$ > 2.5 GeV [25].

Another condition that allow to simplify the description of the reaction is having high momentum transfer in the elementary hN scattering. In this case, one can factorize the hard-scattering process from the soft re-scatterings. Because the momenta of the scattered hadrons are in the order of few GeV/c the latter process can be described using Eikonal approximation.

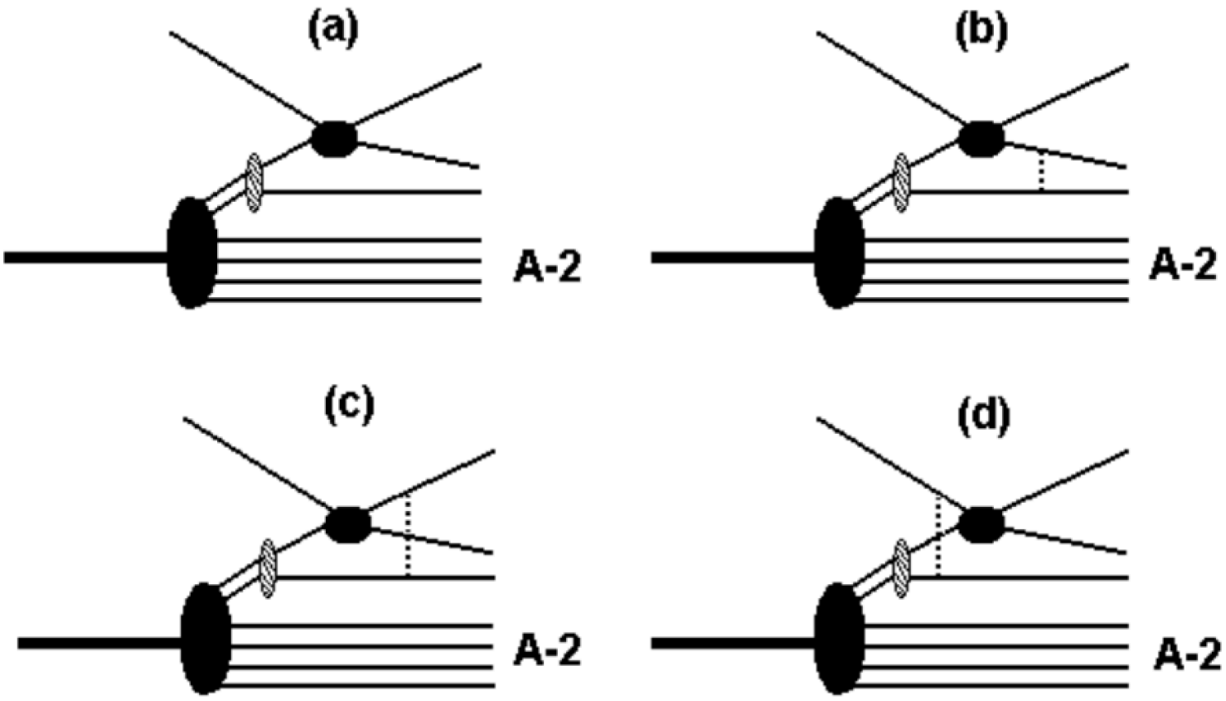

Figure 7: Initial and Final State Interactions (ISI, FSI).

For A(p, 2p)X and A(p, 2pn)X reactions the theoretical analysis of the data will be based on the generalized eikonal approximation (GEA) [26,27,28]. This approximation takes into account multiple interactions of the proton with the NN pair based on the theoretical analysis of the reaction p^{2}H->ppn. Typical diagrams for this reaction are presented in fig.7. The re-interaction with non-correlated nucleons are taken into account within conventional semi-classical models such as described in ref. [29].

Note that in the proposed kinematics all binary invariant energies are large, such that the invariant mass in the intermediate state exceed 2.5 GeV. As we discussed above, this significantly simplifies the theoretical treatment. Also, this kinematics strongly suppress the contribution of the charge exchange two step processes like p^{2}H->ΔNN->ppn. The GEA formalism was tested in the studies of the e^{2}H->pn at Jefferson Lab for large values of bound nucleon momenta relevant to the SRC studies in the nuclei [30].

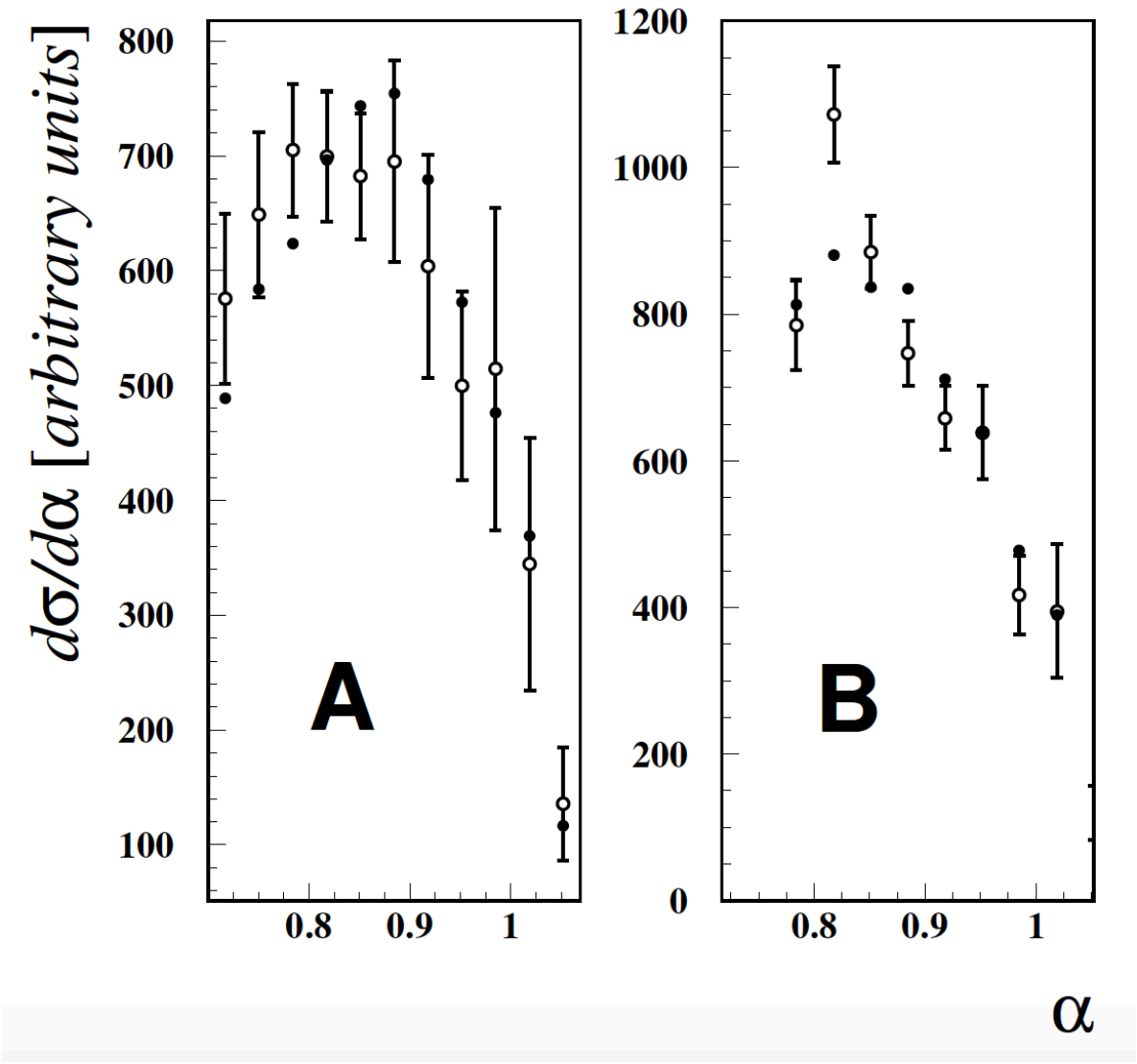

Figure 8: A comparison between calculated α-distributions (solid circles) and the experimental data (open circles) at 5.9 GeV/c (A) and 7.5 GeV/c (B).

The first model for A(p,2p)X and A(p,2pn)X reactions for Carbon nucleus was developed for BNL/AGS energies in which incoming proton momenta were p>6 GeV/c and the nucleus was carbon. These calculations were successfully used for the analysis of the EVA collaboration data. An example of the comparison of EVA/BNL data with the theory is presented in Fig. 8 [23]. This comparison shows rather reasonable agreement with the data for the SRC parameters, which are similar to those extracted in electro-production studies.

We plan to perform calculations for the specific conditions of the proposed measurement. Monte Carlo analysis based on the theoretical calculations will be used to analyze the data in particular to establish kinematics least affected by multiple soft re-scatterings which is

important for extraction of the SRC parameters with minimal modification due to nuclear effects.

2 Experimental Setup

The typical kinematics for scattering off an SRC-pair in the ^{12}C nucleus from a proton in a LH_2 target is shown in fig. 9. A proton (P_{miss}) from the SRC-pair is scattered from a standing proton in the target. After the scattering, the two leading protons have a large angle with respect to each other in the laboratory system. The short-range correlated nucleon emerges forward. The A-2 system moves along the beam direction after the scattering. We plan to detect the leading protons, the A-2 system, and the recoil neutron or proton form np-SRC and pp-SRC pairs, respectively.

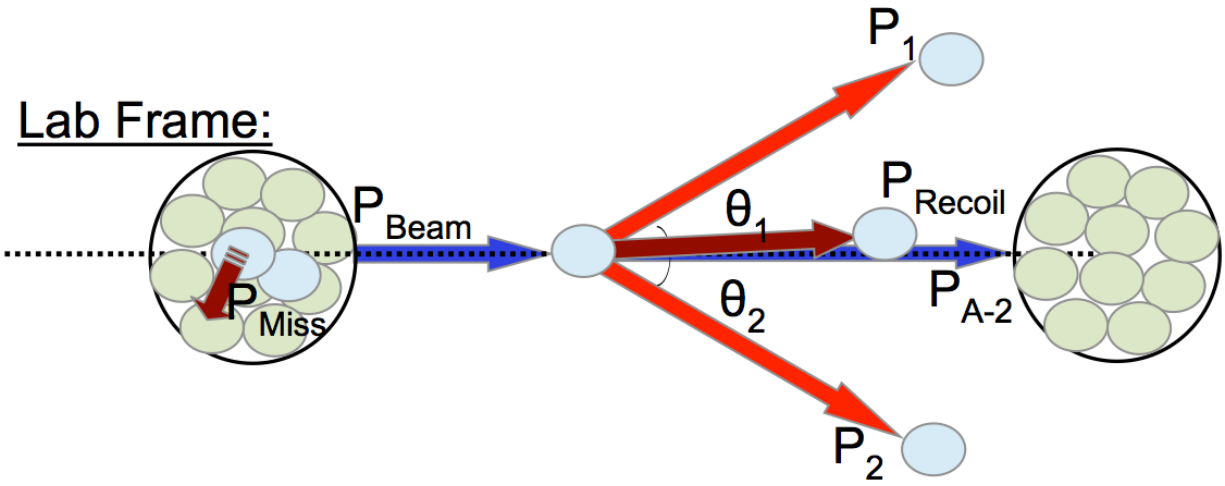

Figure 9: Typical kinematics of hard scattering on a SRC-pair in inverse kinematics. A SRC-proton (P_{miss}) in the nuclear beam knocks a proton (P_2) out of the target. The scattered proton (P_1) has a large angle with respect to the knocked out one. The SRC-correlated partner is moving forward in the LAB (P_{recoil}). The beam remnant nucleus continues with the beam direction (P_{A-2}). See more details in figures 16-17.

A schematic of the proposed experimental setup and details of the target area are shown in figures 10 and 11. The proposed setup is based on the original BM@N layout with some important modifications accounting for the kinematics of the quasi-elastic scattering reaction $^{12}C(p,2p(A-2)p(n))$.

In order to reconstruct the beam direction and monitor the beam position we are planning to use two proportional chambers which will be placed right after the last quadruple lens.. The 30 cm LH_2 target and trigger detectors will be placed after the proportional chambers and right before the horizontal steering magnet SP-57, which will be turned off during our

experiment. The steering magnet VKM will be removed from the beam line to accommodate the proportional chambers and the target ensemble. A scintillator counter read out by an MCP-PMT, placed right before the target, will be used as a start (T0) detector. A plastic scintillator, T_1 will be placed after the target and used for offline separation between the residual (A-1, A-2) systems with different charges. An example of the ability of this detector to separate between nuclei with different charges can be seen in figure 12. Two pairs of scintillator counters (LS1, LS2) will be used as part of the trigger. The trigger is provided by the coincidence of T0 * LS1 * LS2.

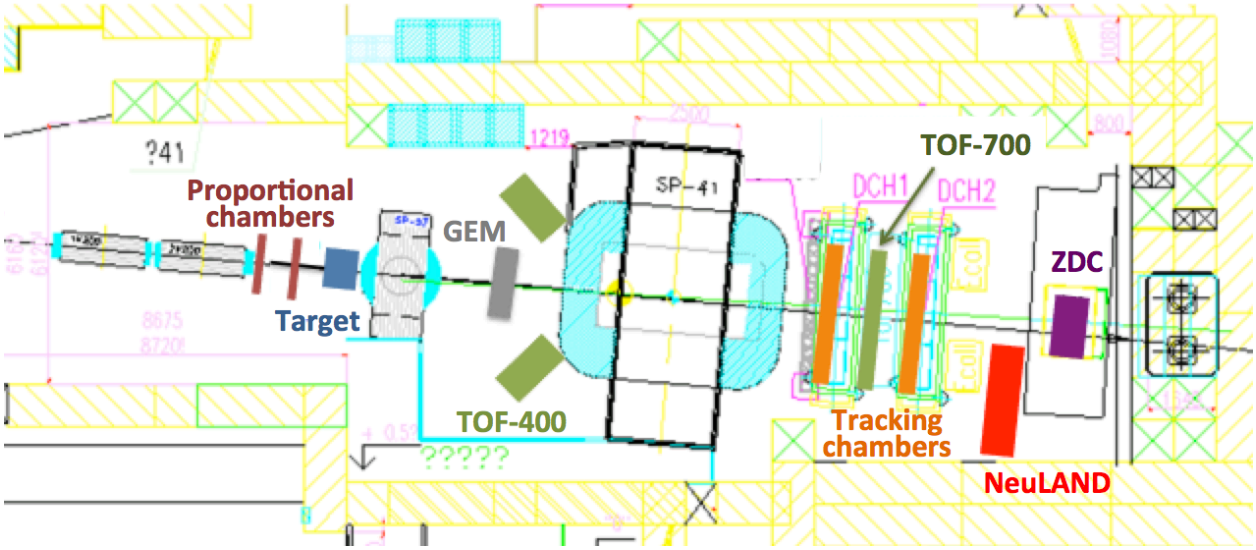

Figure 10: Schematic of the experimental layout.

The leading protons will pass through the trigger scintillator pairs (LS1 and LS2) and then be detected and their time-of-flight be measured by two MRPC walls (TOF-400) with dimensions of 1.15 m x 1.3 m located on both sides of the analyzing magnet SP-41. Between the TOF-400 walls and the LS pairs two GEMs placed side by side having overall dimensions of 80 cm x 66 cm will be used for a precise reconstruction of the polar and azimuthal angle of each leading proton, see figure 11.

The recoil nucleons will have momentum of several GeV/c and will be emitted forward with polar angles up to about 10^{o}. A plastic scintillator T_1 placed right after the beam will be used for offline separation between A-2 systems with different charges. One silicone detector together with one GEM, 40 cm x 66 cm, will track the recoil protons and A-2 system before the SP-41 magnet, and the two DCH stations before and after the TOF-700 will do the track reconstruction downstream the SP-41.

It is important to separate between different A-2 systems. The identification principle for A-2 system is shown in figure 13. By reconstructing trajectory before and after the analyzing magnet, the turning angle can be determined, which, together with the time-of-

flight information measured by TOF-700 at a distance of about 12 m from the target, will help to distinguish between ^{10}B, ^{11}B, and ^{10}Be (see figure 14).

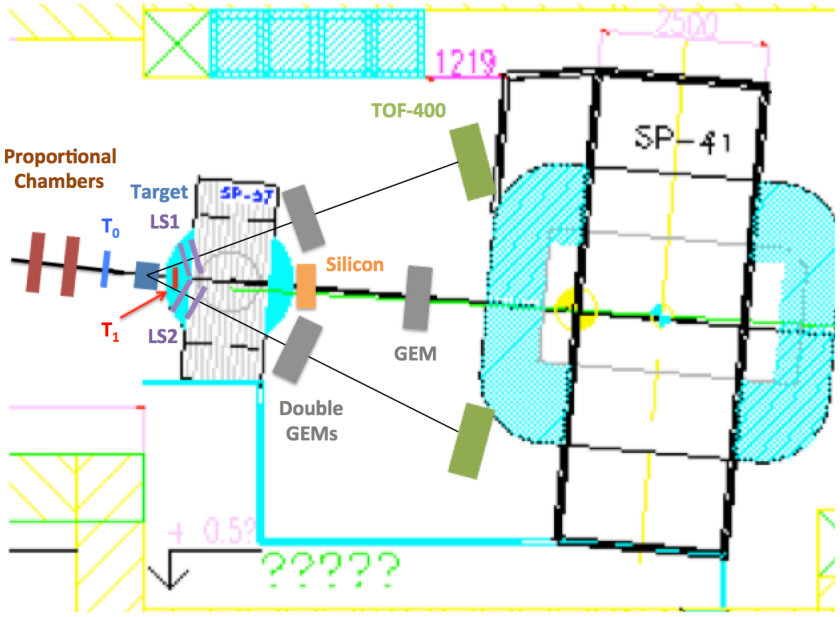

Figure 11: Target ensemble including the liquid hydrogen target and trigger detectors: T_0, two scintillator pairs for the leading protons (LS1 and LS2) that together with T_0 form the trigger. The GEMs placed side by side together with the TOF-400 are used for reconstructing the polar and azimuthal angle of each one of the leading protons. The plastic scintillator T_1 is for offline separation between A-2 systems with different charges.

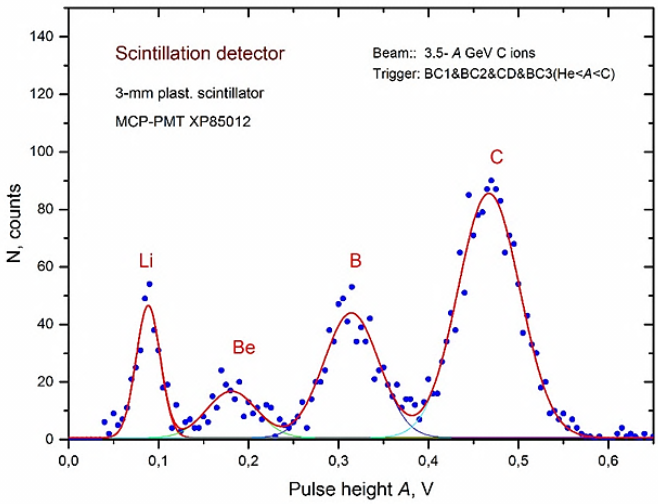

Figure 12: A demonstration of the T_1 detector to separate between nuclei with different charges.

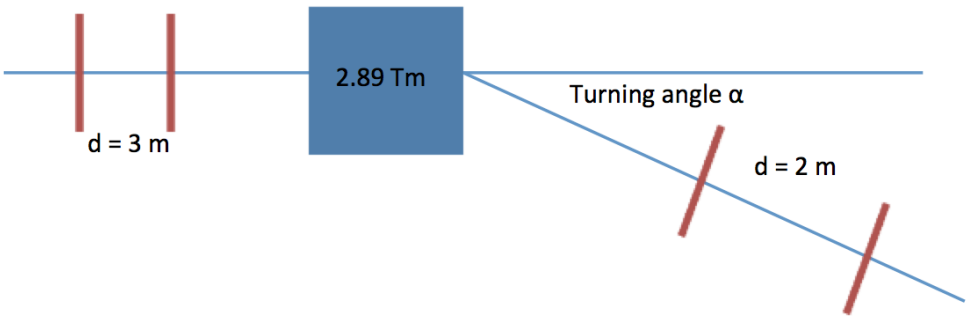

Figure 13: Principle of separation between the expected A-1 and A-2 systems (^{10}B, ^{11}B, and ^{10}Be). The A-2 identification is based on reconstruction of the bending angle using tracking upstream and downstream the analyzing magnet, as well as the time-of-flight information.

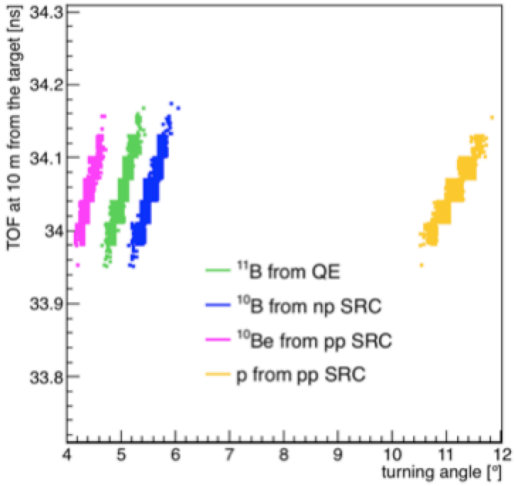

Figure 14: The forward going A-2 system and recoil protons identification using the magnet bend angle and the time-of-flight information. Here the spatial resolution of the tracking chambers is taken into account as well as the timing resolution for the system T0 – TOF-700. A 1% momentum spread is assumed.

The forward going recoil neutrons will be measured with the NeuLAND detector, which will be placed at the right of the beam [31] at a distance of about 14 m from the target. The ZDC will be shifted to the left of the beam to detect the A-2 and a fraction of the recoil nucleons.

The NeuLAND detector (see figure 15) is a new high-precision large-acceptance neutron detector, which will be transported to Dubna from GSI (Germany). It consists of scintillator bars with dimensions of 5 cm x 5 cm x 250 cm arranged in 8 layers with alternating orientation of the scintillators, giving a total thickness of the sensitive area of 40 cm. The sensitive area of the detector is 2.5 m x 2.5 m. The expected efficiency for the neutrons with

momentum of 4-6 GeV/c is about 40%. On average, each high momentum neutron will produce a signal in 5-6 bars, which will allow the reconstruction of its trajectory. NeuLAND detector will allow precise reconstruction of neutron momenta based on the time of flight.

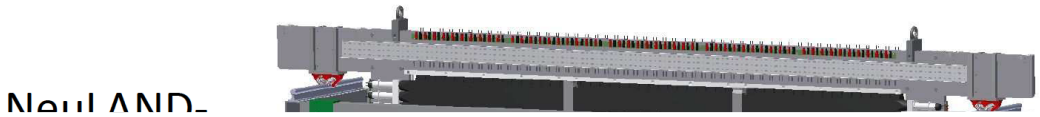

Figure 15: A scintillator plane of NeuLAND together with its support frame.

We plan to use a 4 GeV/c/u carbon beam with an intensity of $3x10^5$ ions/spill and momentum spread of 1% for a net total of two weeks in the next period of operation (November–December 2017). The duty cycle is about 20% with 2 sec slow extraction and a 10 sec total beam cycle. We expect to have a week for preparation of the experiment followed by two weeks of beam time.

3 Simulations and Rate Estimates

To calculate the angle and momentum distributions of the leading protons, the recoil nucleon, and the A-2 system, a proton-nucleus scattering generator is used. The generator starts by calculating the (p,2p) reaction off a nucleon bound in carbon in the carbon rest frame. Next, it boosts to the inverse kinematics frame, hereon referred to as the laboratory (Lab) frame. The kinematical variables are smeared according to the expected resolutions of the detectors and are then boosted back to the carbon rest frame for comparison with their input distributions. The generator conserves energy and momentum in each reaction

vertex. All initial and final state particles are on-shell. The only off-shell nucleon is shown in figure 16 in red.

The initial distribution of nucleons in the nucleus is modeled using a VMC single nucleon momentum distribution based on AV18+UrbanaX interactions [32]. We assume each nucleon with momentum above 0.25 GeV/c is a partner in a SRC pair and describe the SRC pairs using a center-of-mass (c.m.) momentum distribution that is sampled from a 3D Gaussian of width σ=140 MeV/c in each direction [16].

The incident proton beam momentum in the ^{12}C rest frame (figure 17) is calculated by boosting a standing proton 4-momentum vector using a carbon nucleus 4-momentum vector with central momentum of 4 GeV/c/u smeared on an event-by-event basis by 1% in momentum and 0.05^{o} in polar angle to account for the expected uncertainty in the momentum and angle of the Nuclotron carbon beam.

The kinematical distribution of P_1 and P_2 is determined by calculating the (p,2p) reaction in the Center of Mass (C.M.) frame (see figure 17) for a given C.M. scattering angle, θ_{cm}. We consider a C.M. scattering angle range of $\theta_{cm} = 90^{o} \pm 30^{o}$. The A-2 system and recoil nucleon (in the case of scattering off a nucleon in an SRC pair) or the A-1 system (in the case of scattering off a mean-field nucleon) are assumed to be spectators, as indicated by figure 16.

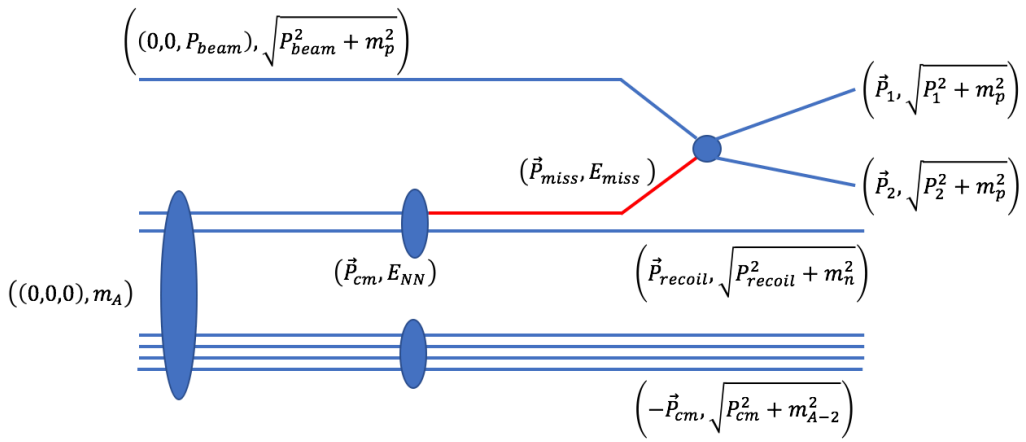

Figure 16: The kinematics for (p,2p) scattering off a proton in a SRC pair inside a nucleus. The off-shell nucleon is marked in red.

The general kinematics for scattering from a nucleon in a SRC pair is shown in figure 17 for the center of mass (C.M.) frame, the ^{12}C nucleus rest frame, and the Lab frame.

The cross section for proton-proton scattering is estimated in the rest frame of proton within the nucleus using the known H(p,2p) differential cross-section [33-37]. Figure 18 shows the cross sections used for $\theta_{cm} = 90^o$. The dependence of the cross-section on the c.m. scattering angle is from ref. [35].

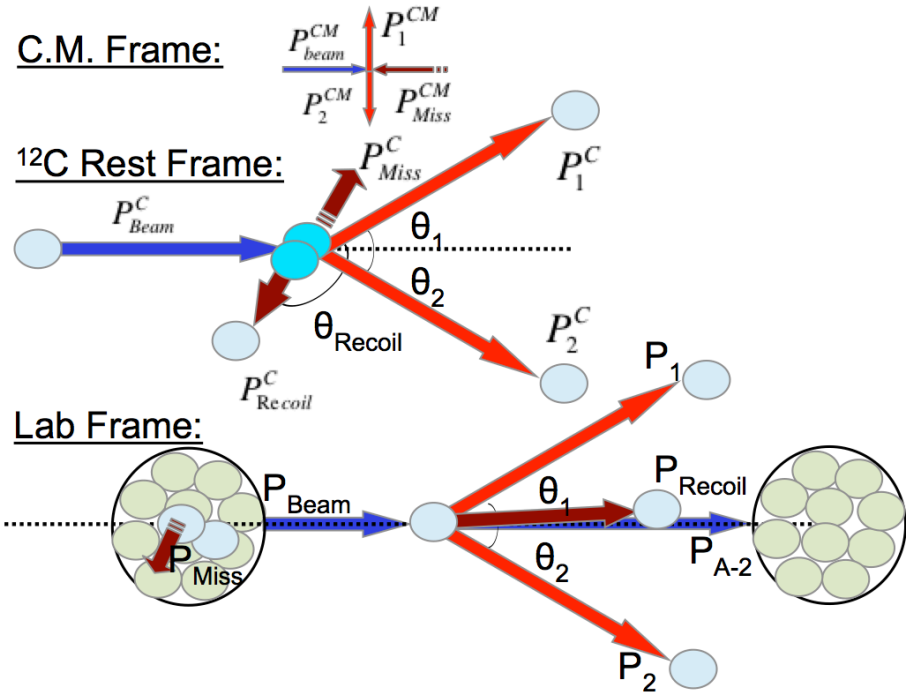

Figure 17: (Top) Two protons scattering at $\theta_{cm} = 90^o$ in their C.M. frame. The momenta of the particles after scattering are P_1(C.M.) and P_2(C.M.). (Middle) Proton beam scattering off an SRC-pair inside a stationary nucleus. The beam proton scatters from a proton within the SRC-pair with initial momentum P_{miss}, knocking it from the nucleus. The short-range-correlated partner recoils backward with momentum P_{recoil}. (Bottom) A SRC-pair in a moving carbon is scattering off of a stationary proton target. A SRC-proton in the carbon nucleus knocked out of the target. The short-range-correlated partner is boosted forward with momentum P_{recoil}. The A-2 nucleus continues along the beam direction (P_{A-2}).

The detectors position was optimized based on the result of the kinematical simulation described above and the physical constraints of the BM@N setup and experimental hall. Events of interest were further constrained to come from hard reactions (i.e. |s, t, u|>2 $(GeV/c)^2$) and kinematics were chosen to select scattering off of nucleons in SRC pairs.

Figure 19 shows the resulting polar angular distribution of P_1 in the laboratory frame. For each leading proton, we placed the trigger detector, the GEMs and the TOF-400 around the mean of this distribution at 31.5°. At a distance of 5 meters from the target, it gives an angular coverage for TOF-400 which is equal to ±6.5° and ±7.5° in polar and azimuthal angles, respectively.

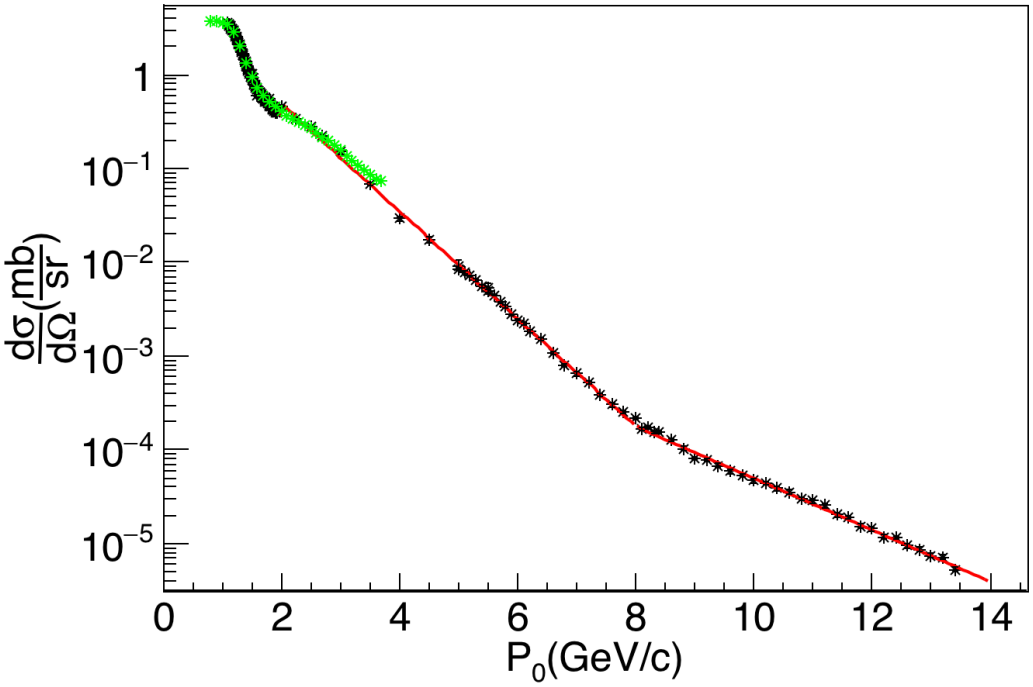

Figure 18: The proton-proton quasi-elastic differential cross sections for $\theta_{cm} = 90^{o}$ (black data points) together with the predictions from SAID model [37] (green points). Five different empirical fits (red curves) are used to fit the data from 1.1-1.2 GeV/c, 1.2-1.6 GeV/c, 1.6-2.0 GeV/c, 2.0-8.0 GeV/c and 8-14 GeV/c. The method of using different empirical fits to describe the pp quasi-elastic differential cross sections in this kinematical region was first used by [34].

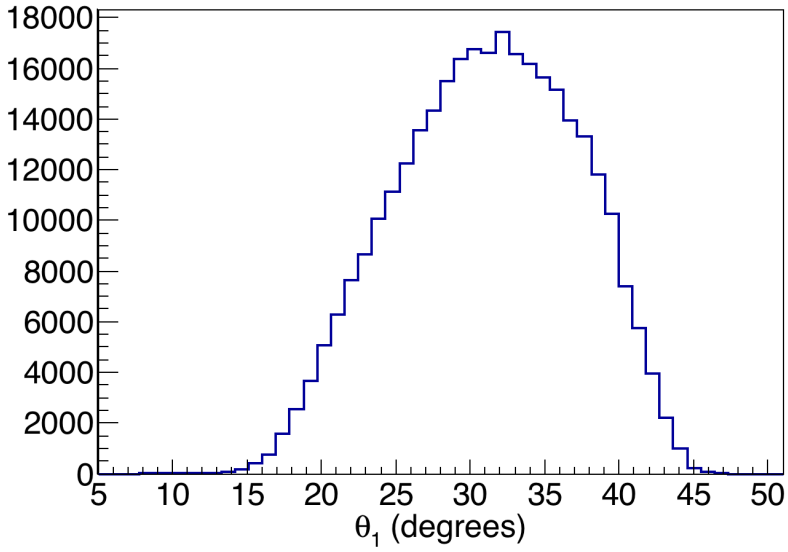

Figure 19: The polar angle distribution of the P_1 proton in the Lab frame.

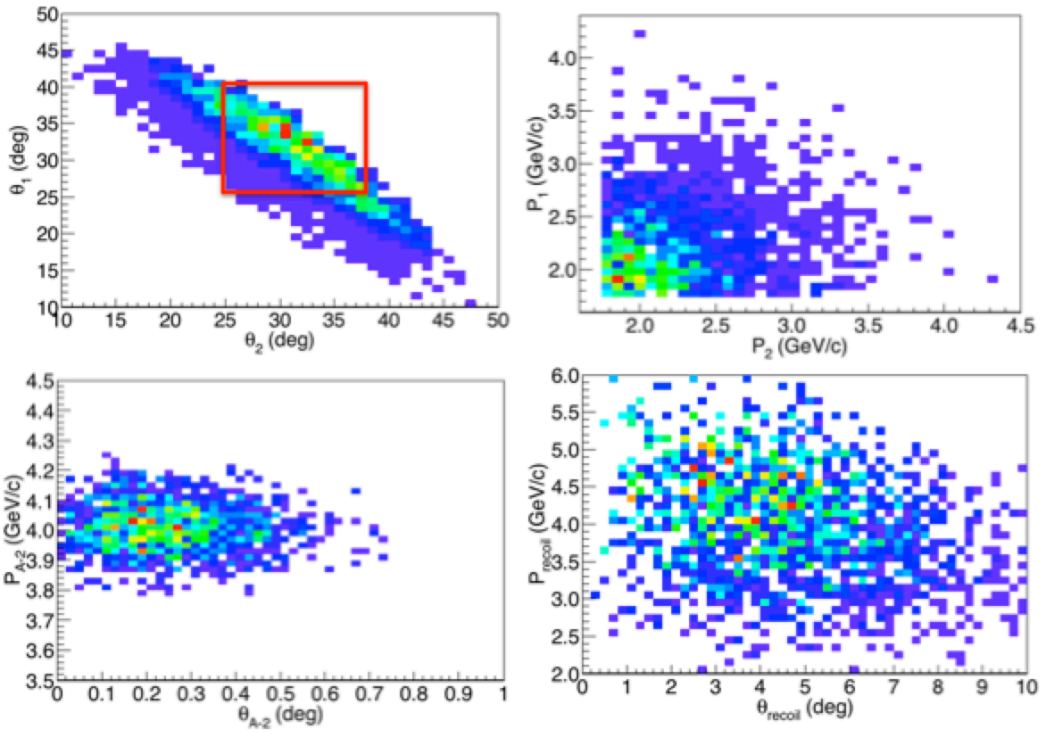

Figure 20: Angular (top, left panel) and momentum (top, right panel) correlation between the two leading protons together with the correlation between the polar angle and the momentum for the A-2 system (bottom, left panel) and the recoil (bottom, right panel). The red box at the top, left panel shows the polar angular acceptance of the TOF-400 detectors.

Figure 20 shows the correlation of the angular and momentum distributions of the two leading protons (top two panels) together with the correlation between the polar angle and the momentum for the A-2 system and the recoil (bottom left and right panel, respectively). The events that are kept correspond to hard scattering events with |s, t, u|>2 $(GeV/c)^2$, initial P_{miss}>0.25 GeV/c, $25° \leq \theta_{1,2} \leq 38°$, $|\varphi_1|$<7.5° and $||\varphi_2|$-180.0°|<7.5°.

From figure 20 above, it is clear that the A-2 system continues mostly undisturbed downstream with a polar angular distribution that does not exceed 1°. Based on these findings, we decided to use one silicon detector, one GEM and the two DCH detectors positioned right before (silicon+GEM) and after (two DCH) the SP-41 analyzing magnet to reconstruct the track of the A-2 nuclei and its turning angle. The turning angle together with its time-of-flight that will be measured by the TOF-700 will help to distinguish between different A-2 systems (Fig. 14).

Based on figure 20, the recoil nucleon (neutron or proton) continues also downstream with a polar angle up to 10^o. NeuLAND detector will be used to detect the recoil neutron, placed on the right of the beam, ~14 m from the target. Part of the recoil nucleons will be also detected the ZDC detector placed on the left of the beam at a distance of about 15 m away from the target.

We smeared the momenta and angular distributions of the P_1, P_2, P_{recoil} and P_{A-2} based on the performance of the detectors that will track and detect them.

The knowledge of the magnitude of the beam momentum and its direction is important for the success of our experiment. Based on previous measurements, the magnitude of the beam momentum can be determined with a precision of 1%. The precise measurement of the incident beam direction requires a pair of proportional chambers, which will be placed before the target 1.0 m apart. These will allow to measure the incident beam direction with angular uncertainty of 0.04^o.

The polar and azimuthal resolutions of the two leading protons will be determined by the combination of GEM and the TOF-400 detector hit position uncertainties. The TOF-400 will be placed 5 m away from the center of the 30 cm LH_2 target with hit position uncertainties of (1.2 cm/$\sqrt{12}$, 6 mm) [38,39]. These resolutions combined with the resolutions of GEMs (0.4 mm, 1.6 mm) [38,39] result into angular resolutions of the proton direction of (0.07^o,0.13^o). The ToF-400 time resolution which will determine the momentum resolution of the two leading protons was previously measured in technical runs with deuteron and carbon beams and was found to be better than ~80 psec [39].

The angular and momentum resolutions of the recoil neutron are determined by the angular and time resolutions of NeuLAND detector. NeuLAND detector will be placed ~14 m away from the center of the 30 cm LH_2 target. The polar and azimuthal resolutions of NeuLAND detector are determined by the dimensions of its scintillator bars 5cm x 5cm x 250cm [31]. Both polar and azimuthal resolutions are estimated to be 0.06^o (=arctan(0.05/$\sqrt{12}$/14)) assuming a uniform distribution for the incident recoil events. The time resolution of NeuLAND was measured by the R^3B collaboration and found to be equal to ~150 psec [31]. A summary of the resolutions used in the generator is listed in Table 1.

Polar and azimuthal resolutions for the A-2 system are based on the resolution of the silicon detector and the GEM situated upstream, and DCH1, DCH2 downstream, of the SP-41 magnet. The spatial resolution of the silicon detector is 0.1 mm while the spatial resolution of the single GEM is as before (0.4 mm, 1.6 mm) [38,39]. The polar and azimuthal resolutions before the SP-41 magnet are 0.007^o and 0.03^o, respectively. The DCH detectors located 2 m apart and after the SP-41 magnet have a spatial resolution of 0.5 mm [38,39] that leads to an uncertainty of 0.02^o. The overall angular resolution is estimated to be 0.04^o.

The A-2 system momentum resolution is defined by the angular resolution uncertainty and the magnitude of the bending angle in the magnet, which is ~5°. The momentum resolution of the A-2 system is calculated to be 0.6%. The reconstruction of the trajectory of the A-2 before and after the analyzing magnet will lead to the determination of its turning angle and momentum, which, together with the time-of-flight information measured by TOF-700 measured with a precision of ~80 psec [39] at a distance of about 11 m from the target, will help to distinguish between A-2 nuclei.

Detectors	Value
Beam Momentum resolution	1%
Beam Angular Resolution	0.04°
TOF-400 time resolution	80 psec
Leading protons polar resolution	0.06°
Leading protons azimuthal resolution	0.13°
NeuLAND time resolution	150 psec
NeuLAND polar resolution	0.06°
NeuLAND azimuthal resolution	0.06°
Momentum resolution for A-2	0.6%
Polar resolution for A-2	0.04°
Azimuthal resolution for A-2	0.04°

Table 1: Expected angular and time resolutions of the detectors relevant for the measurement of the two leading protons (P_1, P_2), the A-2 nucleus, and P_{recoil}.

After smearing all the kinematical distributions in the laboratory frame, we examined the reconstruction of characteristic kinematic variables for identifying the SRC events in the ^{12}C rest frame. An important variable among those is the P_{miss} which is the reconstructed 3-momentum of the struck nucleon before the reaction. P_{miss} can be reconstructed as the sum of momenta P_1 and P_2 minus the beam momentum P_{beam}: $P_{miss}= P_1 + P_2 - P_{beam}$. Figure 21 shows the actual P_{miss} distribution and the reconstructed P_{miss} given the above resolutions.

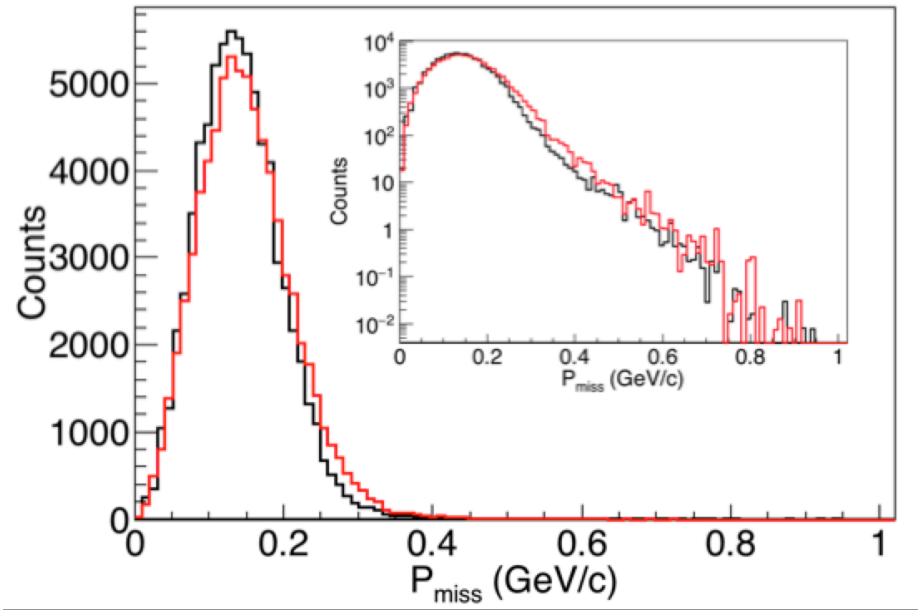

Figure 21: Comparison of simulated(black curve) and reconstructed (red curve) P_{miss} distribution based on the estimated resolutions. Details of the high momentum tails of the distributions can be seen in the insert where both curves are plotted on a logarithmic scale.

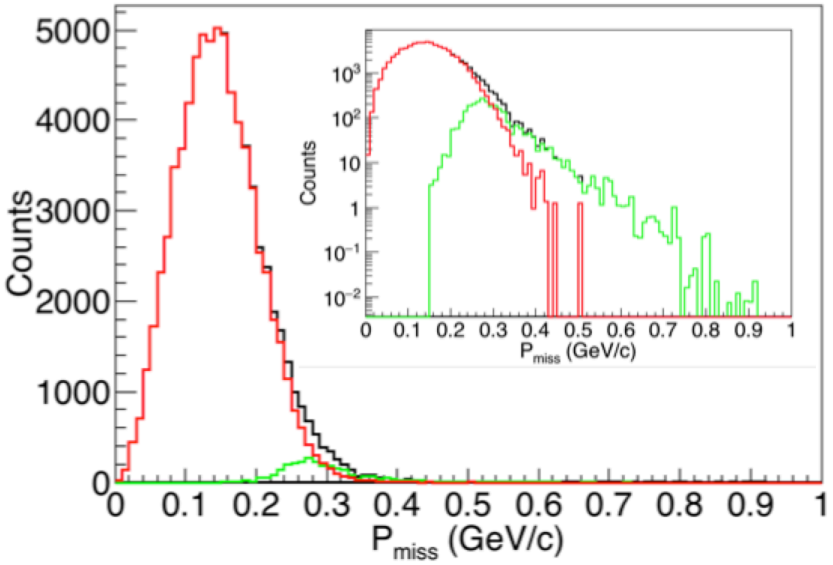

Figure 22 The full reconstructed P_{miss} distribution (black curve) together with the reconstructed P_{miss} for simulated $P_{miss} \leq 0.25$ GeV/c (red curve) and $P_{miss} \geq 0.25$ GeV/c (green curve).

Figure 22 shows the reconstructed P_{miss} distribution and its decomposition to events with original P_{miss} above and below 0.25 GeV/c. The smearing of the initial distribution due to the resolutions of the $P_{1,2}$ momenta leads to the need to identify SRC events by requesting a cut on reconstructed P_{miss} which is higher than 0.35 GeV/c.

The identification of the A-2 system can lead to a large reduction of the mean-field background and consequently to a better SRC identification. This reduction was estimated based on previous measurements [22] to be up to 90%. Figure 23 shows the reconstructed P_{miss} distribution and its decomposition into events with original P_{miss}<0.25 GeV/c scaled down by a factor of 10 and events above 0.25 GeV/c. A cut on the reconstructed P_{miss} above 0.25 GeV/c would ensure the selection of events coming mainly from the SRC-pairs.

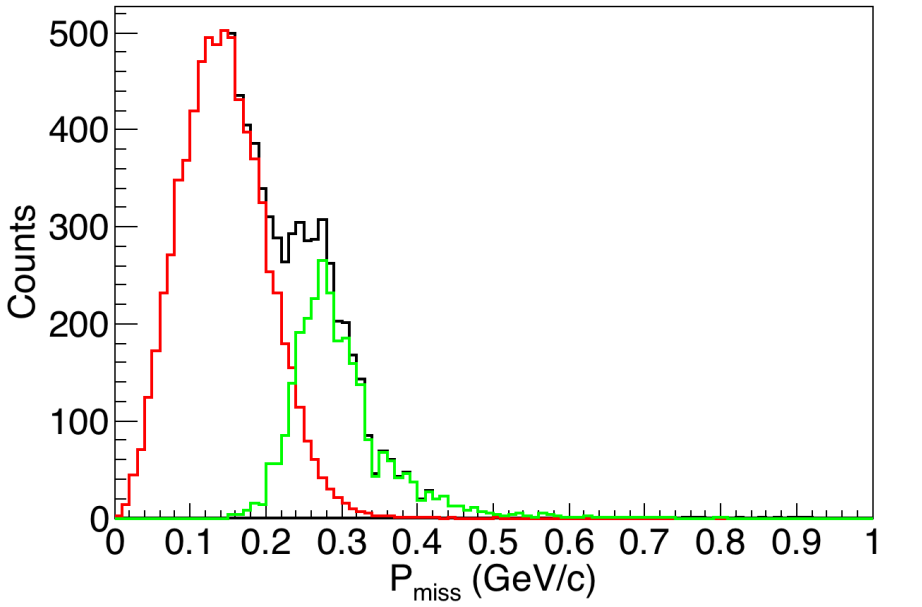

Figure 23 The reconstructed P_{miss} distribution (black curve). Also shown are the reconstructed P_{miss} for events with original $P_{miss} \leq 0.25$ GeV/c (red curve) and $P_{miss} \geq 0.25$ GeV/c (green curve). See text for discussion on the relative contribution of mean field and SRC events assumed in this plot.

In order to calculate the expected yield of events of interest, we assumed that out of the 20% nucleons in SRC pairs, 90% are np pairs and 5% each are pp and nn pairs. The nuclear transparency for the two 1.5 – 3.5 GeV/c leading protons was assumed to be 0.2 [40]. We assumed a 30 cm long LH_2 target (1.2×10^{24} protons/cm^2) and an overall 40% recoil neutron detection efficiency for the 40 cm thick NeuLAND detector. Table 2 summarizes the assumptions made to estimate the yield of SRC events.

Parameters	Values
Target Thickness	1.2×10^{24} protons/cm^2
Beam flux for 4.0 GeV/c	3×10^5 I/s
Beam time	14 days
Duty Cycle	20%
Target Transparency	0.2
Average neutron efficiency	40%

Table 2: A summary of the parameters assumed for the rates estimate.

The cuts used for the selection of the SRC events are listed in Table 3.

Quantities	Cuts
$\theta_{1,2}$ of P_1,P_2	$25° \leq \theta_{1,2} \leq 38°$
φ_1	$\lvert\varphi_1\rvert < 7.5^o$
φ_2	$\lvert\varphi_2 - 180.0^o\rvert < 7.5^o$
|s,t,u|	≥ 2 (GeV/c)^2

Table 3: A summary of the cuts applied in the simulation to estimate the expected measurement rates.

Using the cuts listed in Table 3 and varying the P_{miss} cut as in Table 4 we can calculate the total number of SRC breakup events where two protons are identified by the TOF-400 detectors and assuming identification of the A-1 or A-2 system.

Cut on P_{miss} (GeV/c)	SRC Signal	mean field events
0.25	6347	826
0.275	4693	341
0.3	3022	132
0.325	1770	48
0.35	1255	19
0.375	824	8

Table 4: The expected amount of SRC signal events from the p(^{12}C,2pA-2) reaction in comparison to the corresponding mean field background for different cuts on the reconstructed P_{miss}.

A similar study took place to estimate the expected amount of SRC signal events from the fully exclusive p(^{12}C,2p(A-2)n)X and p(^{12}C,2p(A-2)p)X reactions**.** Figure 25 shows the reconstructed P_{recoil} distribution and its decomposition to events with original P_{miss} above

and below 0.25 GeV/c. A cut at $P_{recoil} \geq 0.30$ GeV/c effectively selects of recoil nucleons coming mainly from the SRC tail.

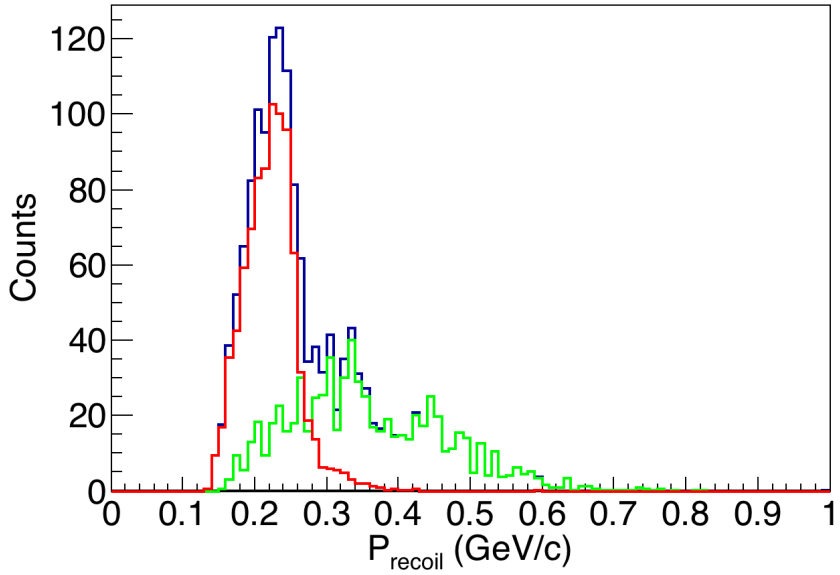

Figure 24 The reconstructed P_{recoil} distribution (**black curve**) shown in red are the reconstructed P_{recoil} with original $P_{miss} \leq 0.25$ GeV/c. $P_{miss} \geq 0.25$ GeV/c are shown in green. A cut at $P_{recoil} \geq 0.30$ GeV/c will select events coming mainly from the SRC tail.

Quantities	Cuts
$\theta_{1,2}$ of P_1,P_2	$25° \leq \theta_{1,2} \leq 38°$
φ_1	$\lvert\varphi_1\rvert < 7.5^o$
φ_2	$\lvert\lvert\varphi_2\rvert - 180.0^o\rvert < 7.5^o$
|s,t,u|	≥ 2 (GeV/c)^2
P_{recoil}	$P_{recoil} > 0.30$ (GeV/c)
x at the plane of z=14 m	0.5 m<x<3 m
y at the plane of z=14 m	1.25 m >y>-1.25 m
z at the back plane of the magnet	z>9 m

Table 5: A summary of the cuts applied in the simulation to estimate the signal rates of the fully exclusive p(^{12}C,2p(A-2)n)X and p(^{12}C,2p(A-2)p)X reactions.

By using the cuts listed in Table 5 and varying the cut on the reconstructed P_{miss} we calculated **the expected number of fully exclusive reactions p(^{12}C,2p(A-2)n)X and p(^{12}C,2p(A-2)p)X in Table 6 and 7, respectively.** There are no simulated mean field events that survive these cuts.

Cut on P_{miss} (GeV/c)	SRC Signal
0.25	445
0.275	347
0.3	244
0.325	158
0.35	121
0.375	86

Table 6: The expected amount of SRC signal events from the exclusive reaction p(^{12}C,2p(A-2)n)X for different cuts on the reconstructed P_{miss}.

Cut on P_{miss} (GeV/c)	SRC Signal
0.25	120
0.275	94
0.3	65
0.325	43
0.35	33
0.375	23

Table 7: Same as Table 6 for the p(^{12}C,2p(A-2)p)X reaction.

3.1 Background Estimation

In order to estimate the background rate of any two charged particles in coincidence that survive the SRC analysis cuts, a total of 100 million events of ^{12}C + p at 4 GeV were generated using QGSM generator [41-46]. QGSM is widely used to describe interactions of light, middle and heavy ions in the Nuclotron energy range. In particular, QGSM generates light nucleus fragments needed to reproduce kinematics of the background processes to SRC [41-46]. The trigger rate can be estimated by applying the geometrical cuts, namely $|\varphi_1| < 7.5^o$, $||\varphi_2| - 180.0^o| < 7.5^o$, $25° \leq \theta_{1,2} \leq 38°$, dictated by the dimensions of the TOF-400 detectors (see top left panel of figure 22). Based on the simulation there are 8976 coincidence events of any two charge particles out of 10^8 proton-Carbon interaction. The coincidences are dominated by the $\pi^{\pm}$ and protons. If the number of ions is $3*10^5$ ions/spill on a target with 6% interaction probability then the amount of background coincidences between the two TOF-400 detectors per spill is ~1.5 events/spill. Therefore, random coincidence triggers are far below the DAQ limit.

The first analysis cut that we can apply to reduce background events while minimizing the loss of signal events is the time-of-flight cut. Figure 27 shows the time-of-flight spectra of the generated particles. A first cut which removes the majority of the $\pi^{\pm}$ is 17.4 nsec <TOF<18.7 nsec. These time-of-flights correspond to proton momenta of 1.75 GeV/c (18.7 nsec) and 2.8 GeV/c (17.4 nsec) and a distance of 5 m. This cut accepts the majority of SRC

events (see top right panel of figure 22) while it rejects fast $\pi^{\pm}$ (see figure 27). 517 out of 10^8 events survive this time-of-flight cut. Figure 28 shows the combination of particles that trigger the system and pass the TOF cut. Primarily, the coincidences are dominated by events where the two particles are $\pi^{\pm}$, $\pi^{\pm}$. However, the number of events with $\pi^{\pm}$, p and p,p is non negligible.

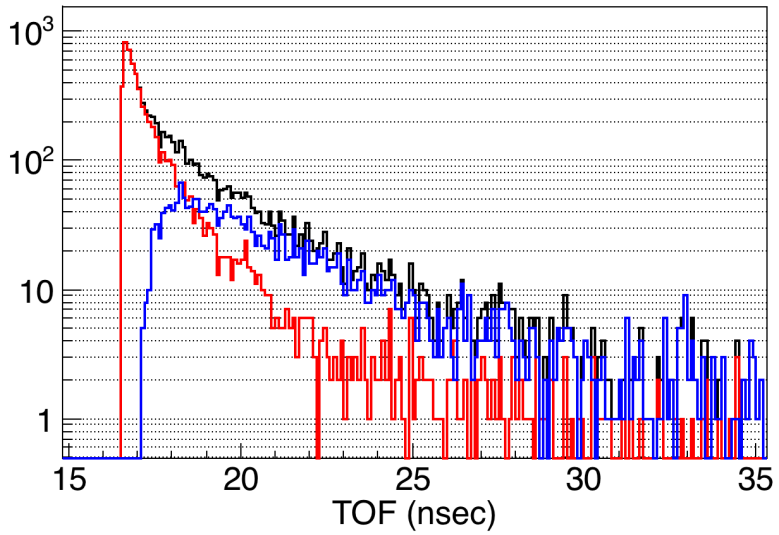

Figure 27 Time of flight spectra of $\pi^{\pm}$ and protons (black), $\pi^{\pm}$ alone (red), and protons alone (blue).

Additional SRC analysis cuts, |s, t, u|>2 $(GeV/c)^2$ and 0.25 (GeV/c)$\leq P_{miss} \leq$1.0 (GeV/c), are applied and reduce the coincidences to 401 out of 10^8 events. In order to reduce the background further we took advantage of the correlations of between the kinematical variables in our signal. These include the polar angles and momenta of the two leading protons. Figure 29 shows the correlation of the polar angles of the two leading protons for the SRC-pair signal (notice that no polar angle cut $25° \leq \theta_{1,2} \leq 38°$ was applied on the events shown in this figure). A graphical cut is applied accepting most of SRC events while reducing the background events to 216 out of 10^8 events.

Figure 30 shows the correlation of the polar angle with the momentum in the laboratory frame for one of the leading protons of the SRC-pairs that survived the first (θ_2,θ_1) cut. A graphical cut (red line) that accepts most of the SRC-pairs is applied. This cut reduces the background events to 96 out of 10^8 events.

The final one-dimensional cut at 5.4 GeV/c < $p_1 + p_2$ < 5.65 GeV/c is applied on the sum of the momenta of the two leading protons in ^{12}C nucleus rest frame. This cut is taking advantage of the narrow peak of the sum of the two momenta p_1+p_2 for the SRC events as

can be seen in figure 31. Adding this one-dimensional cut reduces the background events to $20/10^8$.

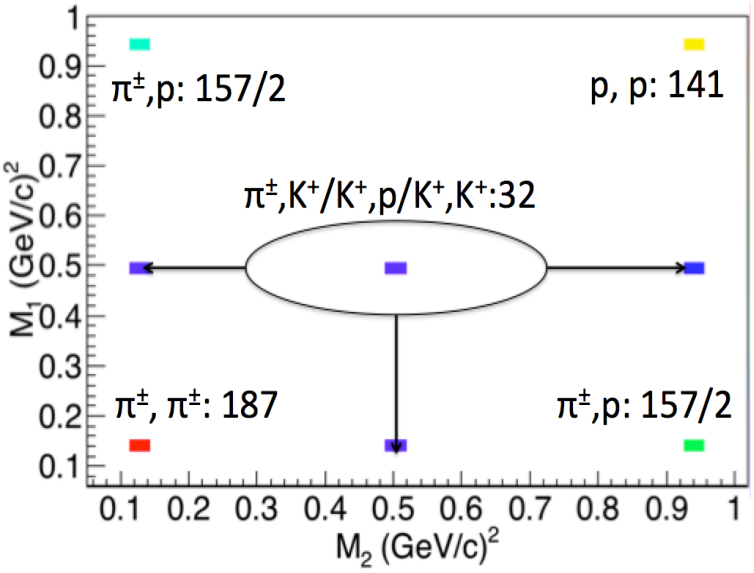

Figure 28 shows the combination of particles that trigger the coincidences and also pass the TOF cut, as a function of their mass.

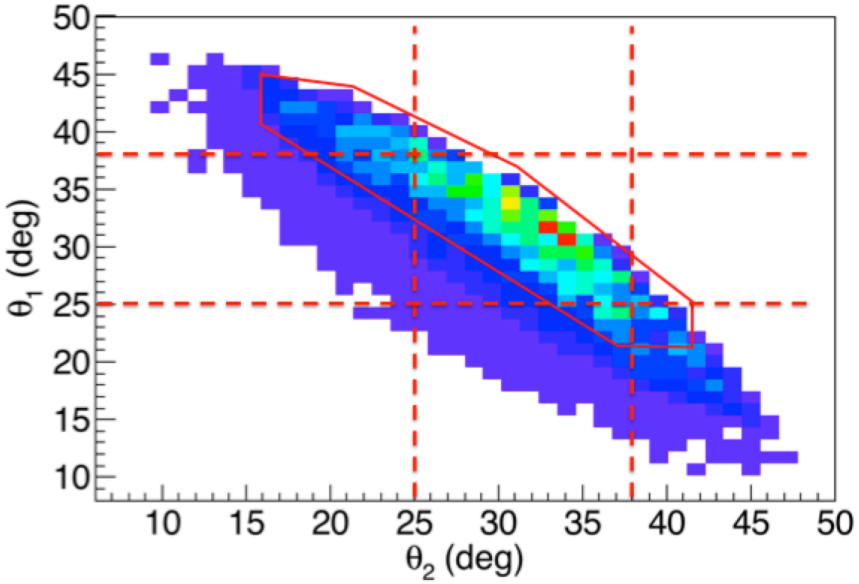

Figure 29 The correlation of the polar angles of the leading protons in the laboratory frame for the SRC signal events. Also shown is the graphical cut (red line) that accepts the majority of the SRC events.

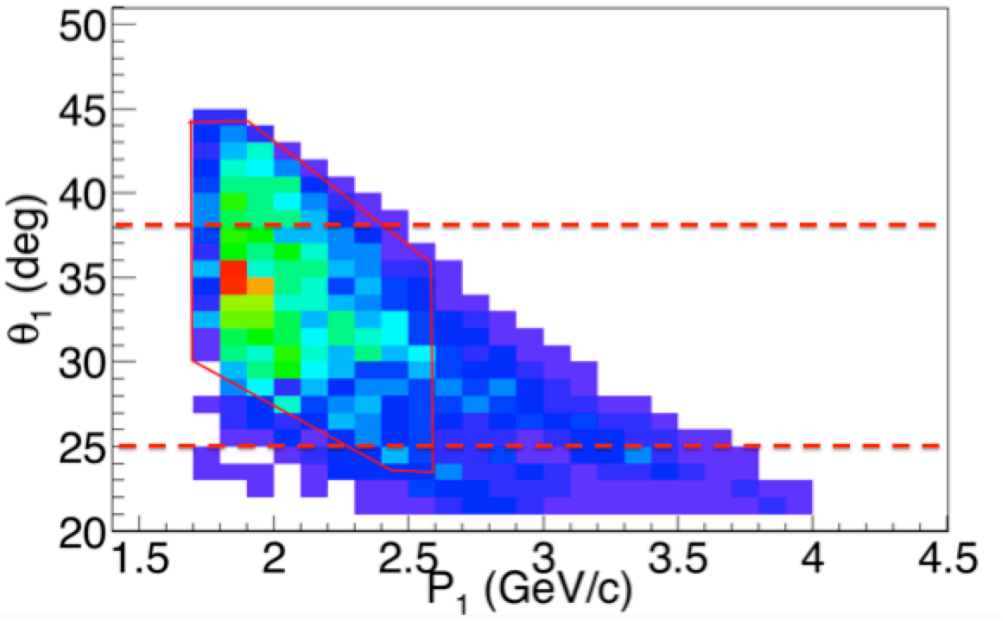

Figure 30 The correlation of the polar angle with momentum for one of the leading protons for the SRC signal together with a graphical cut (red line) that accepts the majority of the SRC events.

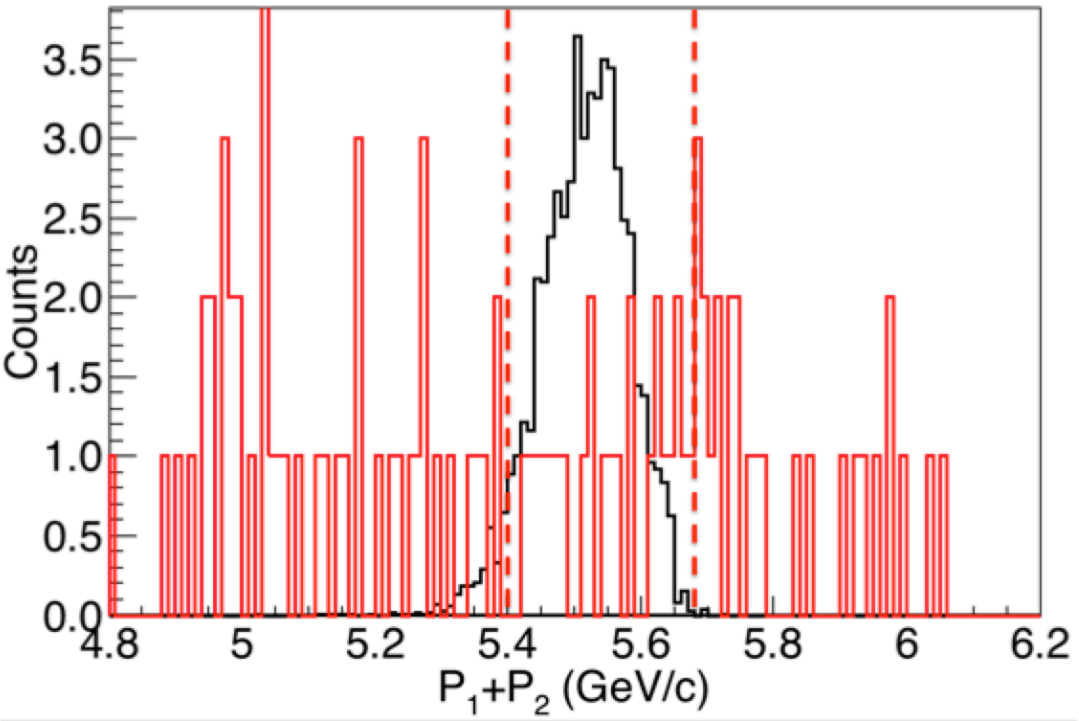

Figure 31 The sum of the momenta p_1+p_2 of the two leading protons for SRC events in the ^{12}C nucleus rest frame (black distribution). The background events are shown in red.

A summary of cuts together with the corresponding event reduction after each cut can be seen in Table 6.

Quantities	Cuts	Counts
$\theta_{1,2}$ φ_1 φ_2	$25° \leq \theta_{1,2} \leq 38°$ $\lvert\varphi_1\rvert < 7.5^o$ $\lvert\lvert\varphi_2\rvert - 180.0^o\rvert < 7.5^o$	8976
$TOF_{1,2}$	17.4 nsec <$TOF_{1,2}$<18.7 nsec	517
|s,t,u| P_{miss}	≥ 2 (GeV/c)^2 0.25 (GeV/c)≤ P_{miss} ≤1.0(GeV/c)	401
$\theta_{1,2}$	2D-cut at (θ_2,θ_1)	216
$\theta_{1,2}$ vs $P_{1,2}$	2D-cut at ($P_{1,2}$,$\theta_{1,2}$)	96
P_1+P_2	5.4 GeV/c < p_1 + p_2 < 5.65 GeV/c	20

Table 8: A summary of the cuts (columns 1,2) and the background events, per 10^8 proton-Carbon interactions, to the p(^{12}C,2p)X reaction that survive after each cut (column 3).

This remaining background of 20 events correspond to a yield of $20/(10^8/6\%) = 1.2\text{x}10^{-8}$ events/incident ^{12}C ion. The yield of the SRC-pairs signal is on average ~3000 events/integrated flux= $4.2\text{x}10^{-8}$ events/ incident ^{12}C ion. The integrated flux = Beam Flux x Time x Duty Cycle = $7.26\text{x}10^{10}$ (see table 2). Based on these yields, the signal to background ratio is expected to be about 4:1. This background should be subtracted from the signal following similar procedures used to analyze the electron scattering experiments.

According to QGSM simulation, only 3 out of the surviving 20 background events contain an A-2 nucleus in the final state. This corresponds to a yield of $3/(10^8/6\%) = 1.8\text{x}10^{-9}$. Assuming that all SRC events will leave a non-fragmented A-2 nucleus, the signal to background ratio for p(^{12}C,2pA-2)X reaction is $4.2\text{x}10^{-8}/1.8\text{x}10^{-9}$ i.e. about 20:1.

Finally, we estimated the background to p(^{12}C,2pn)X reaction. Apart from the cuts described in table 6, additional geometrical cuts are applied to make sure that the neutron contained in the remaining 20 background events will be detected by the NeuLAND detector 14 m away from the target passing through the analyzing magnet. The additional geometrical cuts are given in table 7.

Quantities	Cuts
x at the plane of z=14 m	0.5 m<x<3 m
y at the plane of z=14 m	1.25 m >y>-1.25 m
z at the back plane of the magnet	|z|>9 m
P_{recoil}	0.25 GeV/c<P_{recoil}< 0.7 GeV/c

Table 9 A summary of geometrical cuts applied to the remaining 20 background events for the identification of potential background to **p(^{12}C,2pn)X** reaction.

A total of 1 neutron survive after these geometrical cuts which correspond to background yield of $0.4 \times 1/(10^8/6\%) = 2.4 \times 10^{-10}$. The signal **p(^{12}C,2pn)X** reaction yield estimated to be ~300 events/integrated flux = 0.42×10^{-8}. The signal to background ratio is therefore about 20:1.

3.2 Summary of Event Selection and Expected Results

The expected 2N-SRC yield in two weeks of beam time:

(1) $^{12}C + p \rightarrow {}^{11}B + pp$

(2) $^{12}C + p \rightarrow {}^{10}B + pp$ + X (np-SRC) about 4000 see table 4

(3) $^{12}C + p \rightarrow {}^{10}Be + pp$ + X (pp-SRC) about 4000/20 = 200 events

(4) $^{12}C + p \rightarrow {}^{10}B + pp + n$ (np-SRC) about 350 see table 6

(5) $^{12}C + p \rightarrow {}^{10}Be + pp + p$ (pp-SRC). about 100 see table 7

Estimation of Human Resources

Spokespersons:

Or Hen (MIT), Thomas Aumann (TUD and GSI), Mikhail Kapishin (Dubna), and Eli Piasetzky (TAU),

Coordinators:

Georgios Laskaris (MIT and TAU), Anatoly Litvinenko (Dubna), and Maria Patsyuk (MIT)

The BM@N collaboration

TUD/GSI : Thomas Aumann (PI), Igor Gasparic, and Hans TÃrnqvist ,

MIT: Or Hen (PI), Georgios Laskaris, Maria Patsyuk, and Efrain Patrick Segarra (GS),

TAU: Eli Piasetzky (PI), Erez Choen (GS), Meytal Duer (GS), Igor Korover,

Georgios Laskaris, and Israel Mardor

CAE: Anna Corsi, Alain Gillibert, and Alexandre Obertelli

Appendix

We received comments from Dr. Yuri Uzikov and Dr. Roumen Tsenov. We thank both for their comments that help us to produce this new improved version of the proposal. In this appendix we would like to also refer to these comments in a mode of question/answer.

Comments from Yuri Uzikov:

I would refrain from comments if the names: Misak Sargsian, Mark Strikman, Leonid Frankfurt, were explicitly present in the list of authors. I know them personally.

Misak Sargsian, Mark Strikman, Leonid Frankfurt are now members of the collaboration. Please see chapter 1, section 1.3 for their specific contribution to this proposal that refers to the comments raised below.

The idea to use the inverse kinematics is interesting, as it potentially provides the complete kinematics of the process. The calculations are done in the relativistic dynamics of the light front (I have some experience in it). Probably, also eikonal approximation will be used to account for the nucleons passing through the nucleus.

I have a couple of comments, since I've already started reading the proposal.

1. One of the basic ideas of the project is that the dominant mechanism of the nucleon knock out is a pole diagram (shown in Fig.14 in the proposal), while the second nucleon is a spectator. This mechanism is theoretically justified and works well for large distances between the nucleons in the pair (which corresponds to small relative momenta of the paired nucleons). For decreasing distance (which corresponds to increase of the relative momentum q), it is necessary to account for interaction between the projectile proton with the second nucleon in the pair (since they are overlapping in the short range correlation). We have calculations for the ANKE experiment pd->$(pp)_s$n, which show that re-scattering at moderately large relative momenta q = 0.3-0.6 GeV/c decreases the differential cross section by a factor of 3. We managed to describe the experimental data well only if we account for the interaction between the projectile and the second nucleon in the pair. Please see PLB 562 (2003) 227, Fig. 2b, curves 3 and 4.

   One can probe the interaction of the short range correlation with a proton not only by knocking out one nucleon from the pair back-to-back, but also by picking up one nucleon from the SRC pair into deuteron and detecting the spectator. This process is less probable than the break up of the pair, but it is also more sensitive to the details of the high-momentum component (see ANKE analysis compared to the nucleon knock out with electron probe).

   2. The interaction amplitude between the projectile proton and the struck nucleon is taken on-shell. However, an SRC nucleon is deeply off-mass-shell. And the "off-shell-

ness" increases with the increasing relative momentum of the nucleon in the pair (q). We account for this effect for the ANKE kinematics in the following way: we solve the Schrodinger equation and calculate the partly-2 off-shell amplitude for the pN-scattering based on this solution.

In particular, such partly-off-shell amplitude for pp-scattering for $^1S_0$ state has a node at q = 0.4 GeV/c, which is absent in the on-mass-shell amplitude. Therefore, the partly-o_-shell amplitude and the on-shell amplitude are qualitatively different. For the kinematics of the proposed experiment many partial waves contribute, and the NN potentials are not under control for large q, which makes the calculations difficult. There is an inelastic channel for pN scattering: pN->pN + X, where meson X can be absorbed by the spectator nucleon. This effect would significantly modify the momentum distribution of that nucleon in NN correlation. The triangle diagrams with intermediate mesons X should be taken into account together with the pole diagram with re-scattering (see Yu. Uzikov, J. Haidenbauer, C. Wilkin, PRC 75 (2007) 014008). Strikman and his team does not discuss these effects for p < NN >-interaction.

I'll be glad to discuss it in more detail.

Best regards,
Yuri.

Comments from Roumen Tsenov:

Evaluation report

on the Addendum *"Probing short-range correlations (SRC)"*

to the project *"Studies of baryonic matter at the Nuclotron (BM@N)"*

by **Roumen Tsenov,**

LHEP of the JINR and Sofia University

I was asked by the spokesperson of the BM@N experiment M.N. Kapishin to evaluate briefly and still critically the above Addendum as presented here:

http://bmnshift.jinr.ru/wiki/lib/exe/fetch.php?media=proposal_src_bmn_dubna.pdf
http://bmnshift.jinr.ru/wiki/lib/exe/fetch.php?media=forms_src_24_29.pdf.

Below is my short report.

In this Addendum it is proposed to modify and equip the BM@N set-up with couple of new detectors and perform measurements of certain few body final states created in ^{12}C + p collisions at momentum of 4 GeV/c/nucleon.

Physics motivation stems from the idea that certain part of the nucleons in the atomic nucleus exists in a form of strongly correlated pairs and proposed measurements will shed light on the properties of these pairs and nuclear matter in general. The case is well elaborated in the proposal and enough information is given about the state-of-the-art in the field and what new knowledge will be obtained. Exploitation of inverse kinematics (carbon nucleus bombards proton at rest) moves the particles in the final state in momentum region where they can be successfully identified and their four-momenta measured. This, together with the uniqueness of the Nuclotron beam to perform the measurement is presented convincingly.

The experimental set-up and needed modifications/additions to the BM@N are described with some detail. For better comprehension more info is needed about critical properties of the detectors (resolution, efficiency, etc.), especially for the new ones, or respective references should be given. Table 1 (p. 28) summarizes what has been used in simulation and does not make any reference to experimentally obtained detector characteristics. In addition, using of a liquid hydrogen target in the hall requires some additional work, obtaining of certain permissions, etc., that are not discussed in the proposal.

See chapter 3 for detailed discussion how we obtained the numbers for the resolutions presented in Table 1.

The beam magnitude was measured repeatedly in the past with an uncertainty of 1%. The beam angular resolution is defined by the combined coordinate resolution of $\sigma \sim 1$ mm of a set of two proportional chambers separated by a distance of 1.0 m upstream the target. These determined the incident beam polar angle with resolution of 0.04^{o}.

The ToF-400 spatial resolutions of the strips is (12 mm/$\sqrt{12}$, 6 mm) [38,39]. These resolutions combined with the resolutions of GEMs (0. 4 mm, 1.6 mm) [38,39] determine the polar and azimuthal angular resolutions for the leading protons to be 0.06^{o} and 0.13^{o}, respectively. The ToF-400 time resolution, which defines the momentum resolution of the leading protons, was measured in previous technical runs with deuteron and carbon beams and was found to be better than ~80 psec [39].

The polar and azimuthal resolutions of NeuLAND detector, which determine the resolution of the recoil neutron, are determined by the dimensions of its scintillator bars 5cm x 5cm x 2.5m [31] and the distance to the target (~14 m). Both polar and azimuthal resolutions are estimated to be 0.06^{o} (=arctan(0.05/$\sqrt{12}$/14)). The time resolution of NeuLAND was measured by the R^3B collaboration and found to be equal ~150 psec (which defines the hit location resolution along the 250cm long bars) [31].

Polar and azimuthal resolutions for A-2 system are based on the resolution of the silicon detector and the GEM situated upstream and DCH1, DCH2 placed downstream of the SP-41 magnet. The spatial resolution of the silicon detector is 0.1 mm while the spatial resolution of the single GEM is (0.4 mm, 1.6 mm –see above) [38,29]. The polar and azimuthal resolutions before the SP-41 magnet are 0.007^{o} and 0.03^{o}, respectively. The DCH detectors located 2 m apart and downstream SP-41 magnet have a spatial resolution of 0.5 mm [38,39] that leads to an uncertainty of 0.02^{o}. The overall angular resolution is estimated to be 0.04^{o}.

The A-2 system momentum resolution is defined by the angular resolution uncertainty and the magnitude of the bending angle in the magnet which is $\sim 5^{o}$. The momentum resolution of the A-2 system is calculated to 0.6%. The reconstruction of the trajectory of the A-2 before and after the analyzing magnet will lead to the determination of its turning angle and momentum, which, together with the time-of-flight information measured by TOF-700 measured with a precision of ~80 psec [39] at a distance of about 11 m from the target, will help to distinguish between A-2 nuclei.

Event rate estimate and quality of the expected signal are based on simulations exploiting home-made event generator and by-hand smearing of Monte-Carlo true quantities. The results are questionable as no comparison of the generator with previous measurements is presented. Moreover, some distributions look strange, for example, the black curve in Fig. 21. It should represent, as stated, "actual P_{miss} distribution", i.e. the real one, but a sharp drop-off at P_{miss}=0.25 GeV/c is seen which seems very unnatural.

The generator results were compared with actual data from p + ^{93}Nb reaction acquired by the HADES collaboration at GSI. The simulation reproduces well the data [47].

Instead of using an initial momentum distribution of nucleons in the nucleus that is modeled using a correlated Fermi-Gas model, we used a VMC single nucleon momentum distribution based on AV18+UrbanaX interactions [32]. This model predicts a much smoother transition between the mean field and SRC region. Please see chapter 3 for more details.

Background estimation is not presented convincingly. Identification and tracking efficiencies of the set-up are not given and it is not clear to which extend they have been taken into account. No supporting evidences are given how well the QGSM generator used for "mean-field" background estimation represents the proton-carbon interactions in this energy domain.

QGSM is widely used to describe interactions of light, middle and heavy ions in the energy range of the Nuclotron [41-46]. In particular, QGSM generates light nucleus fragments needed to reproduce kinematics of background processes to SRC. A fully updated estimation of the background based on the QGSM generator is now added in chapter 3 (see section 3.1).

The back-up solution of using CH target instead of liquid hydrogen one is not discussed at all. The background conditions there might be much worse, due to high multiplicity carbon-carbon interactions and this would add considerably to the statistical uncertainty of the subtraction when one tries to extract the carbon-proton signal. Moreover, the time structure of the Nuclotron beam is known to cause triggering on accidentals when one asks for few-fold coincidences and this effect is not discussed, too.

The main option that we consider is the hydrogen target. To suppress the event coincidences on the level of data analysis we plan to use multi-hit TDC to record history of few microseconds for beam and trigger counter signals.

Presentation of the human resources to be involved in the project is superficial. In the supporting form, 120 names are listed. It is absolutely not clear who will really contribute to the project and with what fraction of his/her time (in terms of FTE). Then, a management structure with four (!) spokespersons and three coordinators may work not very efficient and looks strange, to say the least.

BM@N team will cover detector preparation, operation, calibration, data acquisition, triggering, data reconstruction, and calibration. It is difficult to separate these activities in the heavy ion and SRC programs. Most of the BM@N participants will be involved.

Requested resources in terms of money and labor hours in the LHEP workshops seem reasonable. The same is true for the requested beam time with one exception. In my opinion, there is no sufficient time until the next run of the Nuclotron (November-December 2017) for the collaboration to prepare itself for efficient use of the requested 400 hours of beam time there (~17 days). In reality, half of that would be enough for the preliminary measurements they would be prepared for by then and would be able to perform.

400 hours cover all the time needed for the accelerator and beam tuning, failures, refilling of cryogenics, stops due to BM@N. Typical data taking efficiency from the previous run is 65%. We need at least two weeks for data taking to collect the number of events stated in the proposal.

In conclusion, the proposal presents an interesting and perspective physics case, worth of pursuit, but substantial improvements are needed before its presentation to the upcoming PAC end of June 2017.

23.05.2017

Dubna

Roumen Tsenov

e-mail: tsenov@jinr.ru

References

[1] R. Shneor *et al.,* Phys. Rev. Lett. **99**, 072501 (2007).
[2] R. Subedi *et al.,* Science **320**, 1476 (2008).
[3] A. Tang *et al.,* Phys. Rev. Lett. **90**, 042301 (2003).
[4] E. Piasetzky, M. Sargsian, L. Frankfurt, M. Strikman and J. W. Watson, Phys. Rev. Lett. **97**, 162504 (2006).
[5] L. L. Frankfurt and M. I. Strikman, Phys. Rep. **76**, 215 (1981).
[6] L. L. Frankfurt and M .I. Strikman, Phys. Rep. **160**, 235 (1988).
[7] J. Arrington, D. W. Higinbotham, G. Rosner, and M. Sargsian, Prog. Part. Nucl. Phys. **67**, 898 (2012).
[8] R. Schiavilla, R. B. Wiringa, S. C. Pieper, and J. Carlson, Phys. Rev. Lett. **98**, 132501 (2007).
[9] R. B. Wiringa, R. Schiavilla, S. C. Pieper and J. Carlson, Phys. Rev. C **78**, 021001 (2008).
[10] R. B. Wiringa, R. Schiavilla, S. Steven, C. Pieper, and J. Carlson, Phys. Rev. C **89**, 024305 (2014).
[11] I. Korover, N. Muangma, O. Hen *et al.,* Phys.Rev.Lett. **113**, 022501 (2014), arXiv:1401.6138 [nucl-ex].
[12] J. Ryckebusch *et al.,* Nucl. Phys. A**728**, 226 (2003); W. Cosyn, M. C. Martinez and J. Ryckebusch, Phys. Rev. C **77**, 034602 (2008), and W. Cosyn and J. Ryckebusch, private communication.
[13] M. Alvioli *et al.,* Phys. Rev. C **85**, 021001(R) (2012), and C. Cio degli Atti, H. Morita, private communication.
[14] R. Weiss, R. Cruz-Torres, N. Barnea, E. Piasetzky,and O. Hen, "The nuclear contacts and short range correlations in nuclei" , http://arxiv.org/abs/arXiv:1612.00923.
[15] R. B. Wiringa, R. Schiavilla, S. C. Pieper, and J. Carlson, Phys. Rev. C **89**, 024305 (2014).
[16] O. Hen *et al.,* Science **346**, 614 (2014).
[17] M. Sargsian, Phys. Rev. C **89**, 2014, 034305.
[18] L. B. Weinstein, and S. E. Kuhn, "Short Distance Structure of Nuclei: Mining the Wealth of Existing Jefferson Lab. Data", DOE Grant de-sc0006801.
[19] K. Egiyan *et al.,* (CLAS Collaboration), Phys. Rev. C **68**, 014313 (2003), Phys. Rev. Lett. 96, 082501 (2006).
[20] N. Fomin *et al*., Phys. Rev. Lett. **108**, 092502 (2012).
[21] O. Hen, E. Piasetzky, and L. B. Weinstein, Phys. Rev. C **85** (2012) 047301.
[22] V. Panin *et al.,* Phys. Let. B **753** (2016) 204.
[23] I. Yaron, J. Alster, L. Frankfurt, E. Piasetzky, M. Sargsian and M. Strikman, Phys. Rev. C **66**, 024601 (2002).
[24] J. L. S. Aclander *et al.,* Phys. Lett. B **453**, 211 (1999).
[25] L. L. Frankfurt, G. A. Miller, M. M. Sargsian and M. I. Strikman, Phys. Rev. Lett. **84**, 3045 (2000).
[26] L. L. Frankfurt, M. M. Sargsian and M. I. Strikman, Phys. Rev. C **56**, 1124 (1997).
[27] L. L. Frankfurt, E. Piasetzky, M. M. Sargsian and M. I. Strikman, Phys. Rev. C **56**, 2752 (1997).
[28] L. Frankfurt, E. Piasetsky, M. Sargsian and M. Strikman, Phys. Rev. C **51**, 890 (1995).
[29] I. Mardor, Y. Mardor, E. Piasetzky, J. Alster and M. M. Sargsian, Phys. Rev. C **46**, 761 (1992).

[30] W. Boeglin and M. Sargsian, Int. J. Mod. Phys. E **24**, 3, 1530003 (2015).
[31] The R^3B collaboration, Technical Report for the Design, Construction and Commissioning of NeuLAND: The High-Resolution Neutron Time-of-Flight Spectrometer for R^3B, Available at http://www.fair-center.eu/fileadmin/fair/publications_exp/NeuLAND-TDR-Web.pdf [Verified at 06/22/2017]
[32] R. B. Wiringa, R. Schiavilla, Steven C. Pieper, and J. Carlson Phys. Rev. C **89**, 024305 (2014).
[33] C.W Akerlof *et al.,* Phys. Rev. **159**, 1138(1967).
[34] R.C Kammerud *et al.,* Phys. Rev. D **4**,1309(1971).
[35] D.Sivers *et al.,* Physics Reports **1**, 1-121(1976).
[36] M.Garcon *et al.,* Nuclear Physics A **445**, 669(1985).
[37] Institute for Nuclear Studies, The SAID Partial-Wave Analysis Facility, Department of Physics, The George Washington University, available at http://gwdac.phys.gwu.edu [Verified at 06/22/2017]
[38] BM@N collaboration at JINR, available at http://bmnshift.jinr.ru/wiki/lib/exe/fetch.php?media=bmnproject_2016.pdf [Verified at 06/22/2017]
[39] BM@N collaboration at JINR, available at http://bmnshift.jinr.ru/wiki/lib/exe/fetch.php?media=tdr_tof_wall400_22_05_2017_v7.docx [Verified at 06/22/2017]
[40] J. Aclander *et al*., Phys. Rev. C **70**, 015208 (2004), M. Strikman private communication.
[41] A.B. Kaidalov Phys. Lett. B **116**, 459 (1982).
[42] A.B. Kaidalov, K.A. Ter-Martirosyan Phys. Lett. B **117**, 247 (1982); Yad.Fiz. **39**, 1545 (1984) and **40**, 211 (1984).
[43] Yu.M. Shabelsky Yad. Fiz. **44**, 186 (1986).
[44] A. Capella, J. Tran Than Van Phys. Lett. B**114**, 450 (1982); Z.Phys. C **10,** 249 (1981).
[45] P. Aurenche, F.W.Boop, J.Ranft Phys. Lett. B **114**, (1982) 363; Z.Phys. C **13**, 205 (1982). Z.Phys. C **13** 205 (1982) .
[46] X. Artru Phys. Rep. **97** 33 (1983).
[47] The full proposal for the HADES/GSI SRC measurements, available at https://www.hen-lab.com/srchades [Verified at 06/22/2017]